# First-Principles Calculation of $^{17}O$, $^{29}Si$, and $^{23}Na$ NMR Spectra of Sodium Silicate Crystals and Glasses

**Thibault Charpentier***

*Service de Chimie Moléculaire, CEA Saclay, 91191 Gif-sur-Yvette Cedex, France*

**Simona Ispas**

*Laboratoire des Verres, Université Montpellier 2, Place E. Bataillon, 34095 Montpellier Cedex 5, France*

**Mickael Profeta and Francesco Mauri**

*Laboratoire de Minéralogie-Cristallographie de Paris, Université Pierre et Marie Curie, 4 Place Jussieu, 75252 Paris Cedex, France*

**Chris J. Pickard**

*TCM Group, Cavendish Laboratory, Madingley Road, Cambridge, CB3 OHE, United Kingdom*

*Received: September 12, 2003; In Final Form: February 4, 2004*

This paper presents results of first-principles calculations of nuclear magnetic resonance (NMR) parameters: the chemical shielding tensor and the electric field gradient tensor, of some crystalline and amorphous sodium silicate systems. The calculations have been performed using the recently introduced gauge including projector augmented wave (GIPAW) method, which was especially devised for periodic systems. It provides an attractive alternative to the cluster approximation, used in the previous NMR theoretical studies of silicates systems. Moreover, within the GIPAW formalism, amorphous systems can be efficiently described via a supercell approach as demonstrated in this work. Five reference crystalline compounds of known structure (α-quartz, α-cristobalite $SiO_2$, and the sodium silicates $Na_2SiO_3$, α-$Na_2Si_2O_5$, and β-$Na_2Si_2O_5$) and two molecular dynamics models of the sodium tetrasilicate glass $Na_2Si_4O_9$ (NS4) have been studied. The NS4 glass models were generated by a combination of classical and Car-Parrinello molecular dynamics simulations. The good agreement of the simulated $^{29}Si$ MAS NMR and $^{17}O$,$^{23}Na$ 3Q-MAS NMR spectra with the corresponding experimental data demonstrates the accuracy of the GIPAW method. Using these numerically generated data, we have also been able to gain insight into the correlation between NMR parameters and local structural features.

## 1. Introduction

Solid-state nuclear magnetic resonance (NMR) is now a well-established tool for the structural characterization of a wide class of crystalline and amorphous materials such as silicates. NMR is a sensitive and isotopically selective probe of the local environment of atoms and can provide detailed structural information, such as the connectivity, distances, or bond angles with neighboring atoms. Nevertheless, such information cannot be extracted from NMR data without a good understanding of the structural significance of the NMR parameters. This can be achieved either empirically by reference to materials of a known structure or theoretically using ab initio calculations. The first approach has been extensively applied in silicates for $^{29}Si$ NMR,[1] $^{17}O$ NMR,[2−4] and $^{23}Na$ NMR,[5−9] thanks mainly to the development of high-resolution techniques such as magic-angle spinning (MAS) or, for half-integer quadrupolar nuclei, dynamic angle-spinning (DAS), double rotation (DOR), or multiquantum magic-angle spinning (MQMAS). Ab initio calculations in silicates were pioneered by Tossell and co-workers[10−13] for $^{29}Si$ and $^{17}O$ NMR, using model clusters. These calculations have exhibited trends that correlate well with experimental data[14−16] and have been particularly useful in quantifying structural distributions in silicate glasses from NMR data.[17−19] In this context, the major aim of the present study is to improve our ability to connect measured NMR parameters to structural features.

Ab initio NMR shielding and electric field gradient (EFG) tensor calculations of silicates have so far been mostly performed using molecular orbital methods on small clusters[10−13,20−25] modeling the silicate tetrahedral linkage. From experimental observations, the fact that NMR parameters are essentially local properties and are therefore dominated by bonding in the first few coordination spheres is the justification for the cluster approach. Nevertheless, the choice of the correct basis sets for the atomic orbitals remains difficult and this kind of calculation cannot take into account the correlations between the structural factors that exist in solids. Furthermore, calculations of the NMR properties of non bridging oxygens (NBO) or sodiums are much more demanding than those of bridging oxygens (BO), as they require model clusters of a much greater size to achieve sufficient accuracy. Indeed, the cubic scaling with the number of atoms severely limits this kind of calculation. These limitations are certainly the reason so few attempts have so far been

* Corresponding author. Fax: 33 1 69 08 66 40. E-mail: charpent@drecam.saclay.cea.fr.

10.1021/jp0367225 CCC: $27.50 
Published on Web 03/10/2004

**TABLE 1: Mean Values of Some of the Structural Factors of the NS4 Glass Used in the Present Work. (In parentheses are given the standard deviations of each parameter (BO: bridging oxygen; NBO: nonbridging oxygen). The Number of Coordinating Sodium Atoms Has Been Determined as the Number of Sodium Atoms around each Oxygen Atom in a Sphere of 2.95 Å Radius**

| Si−BO Bond Lengths (in Å) (number of coordinating sodium atoms) | | | |
|---|---|---|---|
| $\langle Si-O\rangle_{BO}$ (0 Na) | $\langle Si-O\rangle_{BO}$ (1 Na) | $\langle Si-O\rangle_{BO}$ (2 Na) | $\langle Si-O\rangle_{BO}$ (0 + 1 + 2 Na) |
| 1.609 (0.013) | 1.628 (0.016) | 1.651 (0.023) | 1.619 (0.019) |
| ⟨Si−O−Si⟩ Angles (in degrees) (number of coordinating sodium atoms) | | | |
| ⟨Si−O−Si⟩ (0 Na) | ⟨Si−O−Si⟩ (1 Na) | ⟨Si−O−Si⟩ (2 Na) | ⟨Si−O−Si⟩ (0 + 1 + 2 Na) |
| 147.2 (15.1) | 139.38 (13.4) | 133.8 (13.5) | 143.23 (14.9) |
| Si−NBO Bond Lengths (in Å) | | | |
| $\langle Si-O\rangle_{NBO}$ ($Si:Q^{(2)}$) | $\langle Si-O\rangle_{NBO}$ ($Si:Q^{(3)}$) | $\langle Si-O\rangle_{NBO}$ ($Si: Q^{(2)} + Q^{(3)}$) | |
| 1.566 (0.010) | 1.548 (0.010) | 1.553 (0.012) | |
| Mean ⟨Si−O−T⟩ Angles (in degrees) | | | |
| ⟨Si−O−T⟩ ($Si:Q^{(2)}$) | ⟨Si−O−T⟩ ($Si:Q^{(3)}$) | ⟨Si−O−T⟩ ($Si:Q^{(4)}$) | |
| 145.2 (3.6) | 143.6 (4.6) | 142.9 (6.5) | |
| Na Coordination Number | | | |
| $N_O$ | $N_{BO}$ | $N_{NBO}$ | |
| 4.8 (1.0) | 1.8 (1.4) | 3.0 (1.1) | |
| Na−O Distances (in Å) | | | |
| ⟨Na−O⟩ | $\langle Na-O\rangle_{BO}$ | $\langle Na-O\rangle_{NBO}$ | |
| 2.441 (0.085) | 2.413 (0.985) | 2.353 (0.094) | |

made to calculate $^{23}$Na NMR properties in the silicates.[25] There is therefore a great need of an efficient method for performing NMR parameters (especially the chemical shielding tensor) calculations in periodic systems.

Recently, a new method for the calculation of the NMR chemical shielding tensor in extended systems using periodic boundary conditions has been introduced:[26] the gauge including projector augmented wave (GIPAW) method. It is an extension of the projector augmented wave[27] formalism (PAW) which was successfully applied in the calculation of the electric field gradient.[28] Recent results[29] have shown the good accuracy of the GIPAW method when applied to pure silicates systems, and one purpose of the present work is to pursue such calculations on sodium silicate systems. Our primary objective is to demonstrate that GIPAW can efficiently deal with the large systems required to model amorphous sodium silicates.

In the present work, we first consider five reference crystalline systems of known structure and NMR properties. In addition to determining the few parameters of the GIPAW method, these calculations also serve as a demonstration of the quality of the GIPAW method in predicting NMR properties of sodium silicates. In a second stage, the NMR spectra of two models of the sodium tetrasilicate glass are computed and compared to experimental data. Using these NMR data, some correlations/trends between $^{29}$Si, $^{17}$O, and $^{23}$Na NMR properties and local structures are also investigated.

## 2. Theoretical Methods

**2.1. NMR Chemical Shielding and Quadrupolar Coupling Tensors.** First-principles calculations were performed using the density functional theory (DFT) as applied in plane-wave band-structure calculations. Some of the principles of the computation of the NMR chemical shielding tensor in extended systems using periodic boundary conditions have been described in ref 30, but they were limited in practice to light elements such as $^{13}$C.[31] The GIPAW method[26] removes these limitations, which are due to the use of the pseudopotential approximation. The GIPAW method is an extension of the projector augmented wave (PAW) formalism,[27] and it allows the reconstruction of the all-electron wave function in the presence of a magnetic field. This feature is essential for the accurate computation of the chemical shielding tensor.[28]

**TABLE 2: Parameters Involved in the Construction of the Pseudopotentials for Sodium, Silicon, and Oxygen**

| nucleus | configuration | core radii[a] |
|---|---|---|
| $^{23}$Na | $2s^2\ 2p^6\ 3d^0$ | 1.80 1.49 1.80 |
| $^{29}$Si | $3s^2\ 3p^{1.3}\ 3d^{0.2}$ | 1.99 1.99 1.99 |
| $^{17}$O | $2s^2\ 2p^3$ | 1.45 1.45 |

[a] In atomic unit (au).

In the present calculations, the generalized gradient approximations (GGA)[32] PBE functional is employed. The core electrons are described by norm-conserving Troullier-Martins pseudopotentials,[33] in the Kleinman-Bylander[34] form, generated with parameters given in Table 2. For the GIPAW augmentation, two projectors in each angular momentum channel are used.

For numerical calculations, the plane wave basis set must be truncated and only those plane waves with a kinetic energy smaller than a cutoff energy $E_{cut}$ are kept. Here, a value of $E_{cut} = 100$ Ry has been used, a choice that will be justified later. Integrals over the Brillouin zone are performed using a Monkhorst-Pack *k*-point grid.[35]

Before computing the NMR parameters, the structures (atomic coordinates and lattice parameters) of the sodosilicate compounds $Na_2SiO_3$, α-$Na_2Si_2O_5$, and β-$Na_2Si_2O_5$, were optimized within the DFT framework, in the GGA approximation with the PBE functional. All structures were optimized using a 2 × 2 × 2 Monkhorst-Pack *k*-point grid, and the results are summarized in Table 3 and detailed in the Appendix. As a result, the optimized unit cell volumes overestimate experimental values by about 4.5%. It is well-known that the GGA functional gives a quasisystematic error in bond length which leads to an overestimation of the unit-cell volume. To take this effect into

**TABLE 3: Experimental ($V_{exp}$) and Relaxed ($V_{gga}$) Unit Cell Volumes of the Reference Sodosilicates Crystalline Samples**

| compound | $V_{exp}$ (Å$^3$) | $V_{gga}$ (Å$^3$) | $\Delta V$ (%) | structure |
|---|---|---|---|---|
| $Na_2SiO_3$ | 306.6 | 321.2 | 4.76 | 61 |
| $\alpha$-$Na_2Si_2O_5$ | 483.9 | 505.6 | 4.48 | 62 |
| $\beta$-$Na_2Si_2O_5$ | 471.2 | 491.5 | 4.31 | 63 |

account, the optimized lattice parameters were rescaled so as to span a unit-cell with the experimental volume as described in Table 3. The generation of the NS4 glass models is detailed in section 2.2.

Geometry optimizations of crystalline compounds and NMR calculations were perfomed using the PARATEC code.[36] The program outputs the absolute NMR shielding tensor $\vec{\vec{\sigma}}$ and the traceless electric field gradient (EFG) tensor, in the crystal axis system. Diagonalization provides the principal components (i.e., the eigenvalues) of both tensors. The chemical shielding anisotropy tensor can be computed as well as its relative orientation with the quadrupolar interaction tensor. The isotropic chemical shift $\delta_{iso}$ is obtained from the isotropic chemical shielding $\sigma_{iso} = 1/3\mathbf{Tr}\{\vec{\vec{\sigma}}\}$ through

$$\delta_{iso} = -(\sigma_{iso} - \sigma_{ref}) \tag{1}$$

where $\sigma_{ref}$ is a reference isotropic shielding. Experimentally, the latter is measured on an external reference sample. The chemical shielding tensor can be decomposed into a symmetric $\vec{\vec{\sigma}}^{(s)}$ and antisymmetric part $\vec{\vec{\sigma}}^{(a)}$. The latter can be ignored because NMR is, to first order, not sensitive to this contribution.[37] The anisotropy of the symmetric tensor contribution is then characterized by the chemical shift anisotropy (CSA) $\Delta_{cs}$ reflecting its magnitude and by an asymmetry parameter $\eta_{cs}$ describing its deviation from cylindrical symmetry. These parameters are related to the symmetric shielding tensor through

$$\Delta_{cs} = \sigma_{zz}^{(s)} - \sigma_{iso}, \text{ and } \eta_{cs} = \frac{\sigma_{xx}^{(s)} - \sigma_{yy}^{(s)}}{\sigma_{zz}^{(s)} - \sigma_{iso}} \tag{2}$$

where $\sigma_{xx}^{(s)}$, $\sigma_{yy}^{(s)}$, $\sigma_{zz}^{(s)}$ are the principal components of the symmetric chemical shielding tensor defined such that $|\sigma_{zz}^{(s)} - \sigma_{iso}| \geq |\sigma_{yy}^{(s)} - \sigma_{iso}| \geq |\sigma_{xx}^{(s)} - \sigma_{iso}|$.

Similarly, the quadrupolar interaction is characterized by the quadrupolar coupling constant $C_q$ and the asymmetry parameter $\eta_q$, which are related to the EFG tensor through

$$C_q = \frac{eQV_{zz}}{h}, \text{ and } \eta_q = \frac{V_{xx} - V_{yy}}{V_{zz}} \tag{3}$$

where $V_{xx}$, $V_{yy}$, $V_{zz}$ are the principal components of the EFG tensor defined such that $|V_{zz}| \geq |V_{yy}| \geq |V_{xx}|$ and $Q$ is the nuclear electric quadrupole moment. This quantity cannot be directly measured and is typically derived from experimental $C_q$ values.[38] In the present work, for $^{17}$O and $^{23}$Na, $Q$ was considered as an adjustable parameter.

**2.2. The Tetrasilicate Glass Model.** Concerning the two sodium tetrasilicate (NS4) glass models, we note that each model contains 90 atoms (24 silicon atoms, 54 oxygen atoms and 12 sodium atoms) confined in a cubic box of edge length 10.81 Å corresponding to the experimental NS4 mass density of 2.38 g/cm$^3$.[39] Both glass models have been generated using combined classical and ab initio molecular dynamics (MD) simulations. First, the liquid equilibration, the quench, and the initial part of the low-temperature relaxation were performed within the framework of the classical MD. Subsequently, the obtained structures have been refined within the framework of the ab initio MD. This combined approach was successfully employed for the study of the structural, electronic, and vibrational properties of vitreous $SiO_2$,[40,41] as well as for a structural and electronic study of vitreous NS4.[42,43]

For the classical MD simulations, the interatomic potential that we used is a modified version of the pair potential optimized by Kramer et al.[44] for zeolites and based on ab initio calculations. To use this potential to study sodium silicates, Horbach et al.[45] had to adjusted it so that the charge neutrality is fulfilled in these systems. They introduced for the sodium atoms a distance-dependent charge so as to recover the mass density and the static structure factor of the sodium disilicate glass (more details can be found in ref 45). In previous studies, this potential has been shown to reproduce reliably many structural and dynamic properties of different sodium silicates melts and glasses.[45−48] The two NS4 models were obtained by quenching two different well-equilibrated liquids at 3500 K to 300 K, with the same quench rate equal to $5 \times 10^{13}$ K/s. The glass models obtained this way were relaxed for 70 ps at 300 K. The final configurations (the atomic coordinates and velocities) after the classical relaxations were used as initial configurations for short (≈0.5 ps) ab initio MD simulations. The ab initio simulations were performed within the framework of the Car-Parrinello (CP) method[49,50] using the CPMD software.[51] The technical details of these simulations were identical to the ones described in detail in ref 42, except for the pseudopotential type used for the sodium atoms. During the present CP calculations, we used for the sodium atoms a semi-core Trouiller-Martins norm-conserving pseudopotential[33] instead of the Goedecker semi-core type used previously.[42] This change allowed a better estimation of the internal pressure of the models. Despite this change, both models have presented the same structural modifications as reported in ref 42, i.e., the shortening of the Si−NBO distances and the lengthing of the Si−BO and Na−NBO distances immediately after the CP dynamics was switched on.

At the end of the CP simulations, each NS4 glass model was relaxed to 0 K, using an energy cutoff of 90 Ry for the plane-wave basis expansions of the Kohn−Sham orbitals, while during the CP dynamics we used 70 Ry. Finally, before the NMR calculations, all interatomic distances were rescaled so that the volume of the unit cell is reduced by 4.5%. This rescaling value was deduced from the structural optimization of the reference crystalline compounds, as pointed out in section 2.1. The statistics of some structural parameters characterizing our two models after this rescaling are given in Table 1.

**2.3. Simulation of NMR Spectra.** One- and two-dimensional NMR spectra were simulated using a home-built program, MQSIM.[52] For the quadrupolar nuclei $^{17}$O ($I = 5/2$) and $^{23}$Na ($I = 3/2$), in addition to the static and/or MAS spectra, MQMAS spectra were also simulated. An important feature of MQMAS spectroscopy that should be pointed out is its nonquantitativeness. Indeed, pulsed radio frequency irradiations of the multiquantum transition involved in the MQMAS spectroscopy lead to a strong dependence of the signal intensity with the quadrupole coupling constant (see refs 18, 19). This effect has been taken into account in our simulations, along with more subtle other effects[52] which are beyond the scope of this work. For our purpose, these effects mainly result in a strong attenuation of sites with large quadrupole interaction.

Some of our simulations of NMR spectra will be compared with experimental data obtained on a $^{17}$O-enriched glass of composition ($24SiO_2-76Na_2O$).[53] The different composition with respect to the NS4 glass leads to different relative intensities

**TABLE 4: Convergence of the NMR Parameters for the Sodium Metasilicate $Na_2SiO_3$ ($2 \times 2 \times 2$ *k*-point grid) with Respect to the Cutoff Energy $E_{cut}$ in Rydberg[a]**

| | $^{23}$Na | | | $^{29}$Si | $^{17}$O(1) | | | $^{17}$O(2) | | |
|---|---|---|---|---|---|---|---|---|---|---|
| $E_{cut}$ (Ry.) | $q_{zz}$ | $\eta_q$ | $\sigma_{iso}$ | $\sigma_{iso}$ | $q_{zz}$ | $\eta_q$ | $\sigma_{iso}$ | $q_{zz}$ | $\eta_q$ | $\sigma_{iso}$ |
| 60 | 0.142 | 0.784 | 159.29 | 410.22 | 0.954 | 0.249 | −39.13 | 1.795 | 0.520 | −66.54 |
| 70 | 0.140 | 0.936 | 153.81 | 410.13 | 0.960 | 0.249 | −40.96 | 1.809 | 0.521 | −68.67 |
| 80 | 0.141 | 0.920 | 151.58 | 410.09 | 0.963 | 0.248 | −40.89 | 1.813 | 0.522 | −68.67 |
| 90 | 0.141 | 0.918 | 150.96 | 410.10 | 0.963 | 0.246 | −40.47 | 1.813 | 0.522 | −68.19 |
| 100 | 0.142 | 0.919 | 150.89 | 410.13 | 0.962 | 0.246 | −40.06 | 1.812 | 0.521 | −67.77 |
| 110 | 0.142 | 0.925 | 150.94 | 410.15 | 0.962 | 0.246 | −39.80 | 1.811 | 0.521 | −67.47 |
| 120 | 0.141 | 0.925 | 150.96 | 410.15 | 0.962 | 0.246 | −39.67 | 1.811 | 0.521 | −67.31 |

[a] $q_{zz}$ is the largest in magnitude principal component of the electric field gradient tensor, $\eta_q = (q_{xx} - q_{yy})/q_{zz}$ is the quadrupole asymmetry parameter, and $\sigma_{iso}$ is the isotropic chemical shielding in ppm. The calculations were performed using the experimental structure of the $Na_2SiO_3$.[61]

of NMR peaks but does not affect their spectral features from which NMR parameters are extracted. Further details (preparation of the sample and acquisition of NMR data) are identical to those given in ref 54.

**2.4. Convergence Tests.** In contrast to the molecular orbital method for which the choice of the basis and its convergence properties are rather difficult questions, convergence with respect to plane waves is controlled by only one parameter, the cutoff energy $E_{cut}$. The required value of $E_{cut}$ is controlled by the core radii $r_c$ (one for each angular momentum orbital), given in Table 2. Changing them leads mainly to an overall shift of the theoretical isotropic chemical shifts without changing their relative values. For $^{29}$Si and $^{17}$O, the choice of the pseudopotentials has been discussed in ref 29 and a slightly harder pseudopotential has been chosen in the present work for $^{17}$O. For $^{23}$Na, a harder pseudopotential with $r_c(2p) = 1.24$ au has also been considered, but did not provide significant improvement, as compared to errors typical of NMR measurements.

The convergence tests of our NMR calculations were perfomed on the $Na_2SiO_3$ and α-$Na_2Si_2O_5$ experimental structures using a $2 \times 2 \times 2$ *k*-point grid. The same convergence behavior was observed for both compounds, and the results are given in Table 4 for the metasilicate structure.

Compared to errors typical in NMR measurements which provide $C_q \pm 0.1$ MHz, $\eta_q \pm 0.05$, and $\delta_{iso}$ from $\pm 0.2$ ($^{29}$Si) to $\pm 2$ ppm ($^{17}$O,$^{23}$Na), a value of $E_{cut} = 100$ Ry is entirely satisfactory.

A second convergence criterion that must be checked is the sampling of the Brillouin zone. The latter is strongly dependent upon the size of the unit cell under consideration. The quadrupolar coupling constant and quadrupolar asymmetry parameter are the less demanding parameters with respect to the number of *k*-points, and for the present work, a $2 \times 2 \times 2$ sampling gave converged results with sufficient accuracy. However, for the chemical shielding tensor, a $4 \times 4 \times 4$ sampling was necessary. For the glass samples, the large size of the unit supercell ensures that a single Baldereschi point is sufficient. A calculation using a second point of the $2 \times 2 \times 2$ Monkhorst-Pack *k*-grid confirmed this choice.

## 3. Results

**3.1. The Crystalline Compounds.** Calculated $^{29}$Si, $^{17}$O, and $^{23}$Na NMR parameters are presented in Tables 5, 6, and 7 along with experimental data, and displayed in Figures 1, 2, and 3, respectively. Each site is labeled according to the references given in Table 3.

The computation of the isotropic chemical shift according to eq 1 would require calculations on systems (i.e., standard external reference such as TMS for $^{29}$Si, tap water for $^{17}$O, and 1 M aqueous NaCl for $^{23}$Na) too much different than the silicates of interest. As, from a chemical point of view, the relevant parameter is the isotropic chemical shift difference between different compounds, the reference isotropic chemical shift $\sigma_{ref}$ was computed in order to get the best fit with experimental data. The values were therefore obtained from linear fits of the theoretical isotropic chemical shielding with the constraint of unity slope as shown in Figures 1, 2, and 3 for $^{29}$Si, $^{17}$O, and $^{23}$Na, respectively. We obtained the following values: 334.40 ppm for $^{29}$Si, 259.32 ppm for $^{17}$O, and 173.72 ppm for $^{23}$Na.

For the computation of the quadrupolar coupling constant $C_q$, the value of the nuclear quadrupole moment $Q$ were also needed. Matching the experimental quadrupolar coupling constants yielded the values $Q = 2.50 \times 10^{-30}$ m$^2$ for $^{17}$O and $Q = 9.56 \times 10^{-30}$ m$^2$ for $^{23}$Na, which are very close to the latest *experimental* values[38] of $Q = 2.55 \times 10^{-30}$ m$^2$ (less by 2%) and $Q = 10.4 \times 10^{-30}$ m$^2$ (less by 8%). We used these optimal values to compute the quadrupolar coupling constant (eq 3). For comparison, in previous works values of $Q = 2.23 \times 10^{-30}$ m$^2$ and $Q = 12.25 \times 10^{-30}$ m$^2$ were used for $^{17}$O[11] and $^{23}$Na,[25] respectively.

**TABLE 5: Experimental and Calculated $^{29}$Si Isotropic Chemical Shifts**

| | | experimental | theoretical | | |
|---|---|---|---|---|---|
| compound | $^{29}$Si site | $\delta_{iso}$ (ppm) | $\delta_{iso}$[a] (ppm) | $\sigma_{iso}$ (ppm) | ref |
| $Na_2SiO_3$ | $Q^2$ | −76.8 ± 0.2 | −75.05 | 409.45 | 5 |
| α-$Na_2Si_2O_5$ | $Q^3$ | −94.2 ± 0.2 | −94.88 | 429.28 | 5 |
| β-$Na_2Si_2O_5$ | $Q^3$-Si(1) | −86.3 ± 0.2 | −85.85 | 420.25 | 5 |
| β-$Na_2Si_2O_5$ | $Q^3$-Si(2) | −88.2 ± 0.2 | −87.64 | 422.04 | 5 |
| $SiO_2$(α-cristobalite) | $Q^4$ | −109.1 ± 0.2 | −109.81 | 444.21 | 64, 65 |
| $SiO_2$(α-quartz) | $Q^4$ | −107.0 ± 0.2 | −107.88 | 442.28 | 66 |

[a] $\delta_{iso} = -(\sigma_{iso} - \sigma_{ref})$ with $\sigma_{ref} = 334.40$ ppm (see Figure 1).

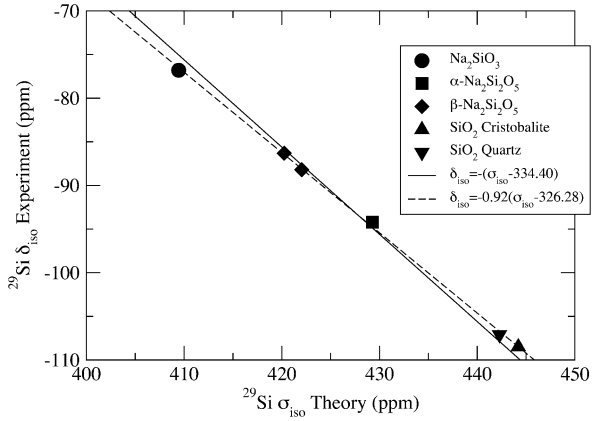


**Figure 1.** Experimental $^{29}$Si isotropic chemical shift $\delta_{iso}$ versus theoretical isotropic chemical shielding $\sigma_{iso}$. The lines are linear fits, the solid line is of unity slope.

**TABLE 6: Experimental and Theoretical $^{17}$O NMR Parameters of the Crystalline Compounds Studied in This Work**

| | | theoretical | | | | experimental | | | |
|---|---|---|---|---|---|---|---|---|---|
| compound | $^{17}$O site | $\sigma_{iso}$ (ppm) | $\delta_{iso}$[a] (ppm) | $C_q$[b] (MHz) | $\eta_q$ | $\delta_{iso}$ (ppm) | $C_q$ (MHz) | $\eta_q$ | ref |
| $Na_2SiO_3$ | BO,O(2) | 191.41 | 67.91 | 4.46 | 0.52 | 63 ± 2 | 4.20 ± 0.2 | 0.58 ± 0.05 | 24 |
| | NBO,O(1) | 220.03 | 39.28 | 2.36 | 0.23 | 39 ± 2 | 2.43 ± 0.1 | 0.17 ± 0.05 | 24 |
| α-$Na_2Si_2O_5$ | BO,O(1) | 216.60 | 42.72 | 5.39 | 0.13 | 55 ± 5 | 5.70 ± 0.3 | 0.00 ± 0.2 | 4 |
| | | | | | | 52 ± 10 | 5.74 ± 0.2 | 0.2 ± 0.1 | 16 |
| | BO,O(2) | 207.38 | 51.94 | 4.83 | 0.37 | 55 ± 2 | 4.70 ± 0.2 | 0.25 ± 0.2 | 4 |
| | | | | | | 74 ± 10 | 4.67 ± 0.2 | 0.3 ± 0.1 | 16 |
| | NBO,O(3) | 227.21 | 32.11 | 2.32 | 0.22 | 34 ± 1 | 2.35 ± 0.1 | 0.10 ± 0.1 | 4 |
| | | | | | | 36 ± 2 | 2.40 ± 0.1 | 0.3 ± 0.1 | 16 |
| β-$Na_2Si_2O_5$ | BO,O(1) | 201.30 | 58.02 | 4.68 | 0.12 | | | | |
| | BO,O(2) | 203.81 | 55.51 | 4.77 | 0.41 | | | | |
| | BO,O(3) | 203.55 | 55.77 | 4.67 | 0.42 | | | | |
| | NBO,O(4) | 230.02 | 29.30 | 2.43 | 0.16 | | | | |
| | NBO,O(5) | 225.97 | 33.35 | 2.13 | 0.06 | | | | |
| $SiO_2$(α-cristobalite) | BO | 222.08 | 37.24 | 5.32 | 0.14 | 36.7 ± 2 | 5.3 ± 0.2 | 0.125 ± 0.05 | 64 |
| | | | | | | 37.5 ± 2 | 5.35 ± 0.1 | 0.21 ± 0.05 | 65 |
| $SiO_2$(α-quartz) | BO | 217.95 | 41.37 | 5.35 | 0.12 | 43 ± 2 | 5.21 ± 0.2 | 0.19 ± 0.05 | 65 |

[a] $\delta_{iso} = -(\sigma_{iso} - \sigma_{ref})$ with $\sigma_{ref} = 259.32$ ppm. [b] Calculated with $Q = 2.50 \times 10^{-30}$ m$^{-2}$.

**TABLE 7: Experimental and Theoretical $^{23}$Na NMR Parameters**

| | | theoretical | | | | experimental | | | |
|---|---|---|---|---|---|---|---|---|---|
| compound | $^{23}$Na site | $\sigma_{iso}$ (ppm) | $\delta_{iso}$[a] (ppm) | $C_q$[b] (MHz) | $\eta_q$ | $\delta_{iso}$ (ppm) | $C_q$ (MHz) | $\eta_q$ | ref |
| $Na_2SiO_3$ | Na(1) | 525.71 | 24.12 | 1.35 | 0.82 | 22.1 ± 0.5 | 1.40 ± 0.1 | 0.7 ± 0.1 | 24 |
| | | | | | | 22.75 ± 0.1 | 1.46 ± 0.05 | 0.71 ± 0.05 | 6 |
| α-$Na_2Si_2O_5$ | Na(1) | 532.49 | 17.34 | 1.78 | 0.95 | 16.9 ± 1.0 | 1.79 ± 0.1 | 1.0 ± 0.05 | 5 |
| | | | | | | 17.4 ± 0.1 | 1.82 ± 0.05 | 1.0 ± 0.05 | 6 |
| β-$Na_2Si_2O_5$ | Na(1) | 534.87 | 14.96 | 2.28 | 0.86 | 15.6 ± 1.5 | 2.29 ± 0.1 | 0.85 ± 0.05 | 5 |
| | | | | | | 20.4 ± 0.1 | 2.50 ± 0.05 | 0.0 ± 0.05 | 6 |
| | Na(2) | 542.25 | 7.58 | 2.25 | 0.56 | 9.4 ± 1.5 | 2.20 ± 0.1 | 0.55 ± 0.05 | 5 |
| | | | | | | 8.3 ± 0.1 | 2.22 ± 0.05 | 0.55 ± 0.05 | 6 |

[a] $\delta_{iso} = -(\sigma_{iso} - \sigma_{ref})$ with $\sigma_{ref} = 173.72$ ppm. [b] Calculated with $Q = 9.56 \times 10^{-30}$ m$^2$.

**TABLE 8: Experimental and Theoretical $^{29}$Si Chemical Shift Anisotropy Parameters of the Crystalline Compounds Studied in This Work**

| | | experimental | | theoretical | | |
|---|---|---|---|---|---|---|
| compound | $^{29}$Si site | $\Delta_{cs}$ ppm | $\eta_{cs}$ | $\Delta_{cs}$ ppm | $\eta_{cs}$ | ref |
| $Na_2SiO_3$ | $Q^2$ | 76.0 ± 10 | 0.7 ± 0.3 | 80.5 | 0.5 | 24 |
| α-$Na_2Si_2O_5$ | $Q^3$ | 93 | 0.28 | 67.5 | 0.1 | 55 |
| β-$Na_2Si_2O_5$ | $Q^3$ | 103 | 0.28 | 75.0 | 0.0 | 55 |
| β-$Na_2Si_2O_5$ | $Q^3$ | 95 | 0.32 | 67.8 | 0.1 | 55 |

As shown in Figures 1, 2, and 3, these calculations demonstrate the good accuracy of the GIPAW method. Notice that for the $^{17}$O isotropic chemical shifts (Figure 2), however, the theoretical values of α-$Na_2Si_2O_5$ are those that deviate most from the experimental data. But it is worth noticing that these data have rather large uncertainties resulting from the high complexity of the experimental spectra (the lines strongly overlap), and moreover, we think that these uncertainties are underestimated. As a consequence, the value $\sigma_{ref} = 259.32$ ppm which were obtained by ignoring the α-$Na_2Si_2O_5$ BO data, (dotted line in Figure 2) has been considered in the remainder of this work. This choice also yielded a significant improvement of the agreement between simulated NS4 $^{17}$O NMR spectra with experimental data (see next section). $^{23}$Na data from ref 6 have also not been taken into account in Figure 3 because their NMR spectra[55] display much less well-defined singularities than those reported in ref 5. This has lead, from our point of view, to a wrong determination of the $^{23}$Na NMR parameters for β-$Na_2Si_2O_5$. Is is clear that for this compound the $^{23}$Na NMR spectrum is ambiguous and new measurements should be carried out using advanced high-resolution techniques such as MQMAS.

Due to the lack of experimental results, only the $^{29}$Si chemical shift anisotropy (CSA) parameters of $^{29}$Si are presented in Table 8. For $Na_2SiO_3$, our calculations agree very well with the measurements of Clark et al.[24] Concerning the other experimental data,[55] no uncertainties were given in their work. But taking into account the method they used to extract these parameters and the signal-to-noise ratio of their experimental spectra (somewhat similar to that of ref 24), the uncertainties can be considered to be the same. Thus, our predictions are in rather good agreement with their data.

**3.2. The NS4 Glass.** *3.2.1. Silicon-29.* The $Q^{(n)}$ contributions of the two NS4 glass models are given in Table 9. Comparison with percentage contributions as measured by NMR[56,57] shows the reliability of our theoretical models for this study.

Figure 4 is a plot of the $^{29}$Si isotropic chemical shift $\delta_{iso}$ against the chemical shift anisotropy $\Delta_{cs}$ (left) and the asymmetry parameter $\eta_{cs}$ (right). The $\delta_{iso}$ ranges of $Q^{(3)}$ and $Q^{(4)}$ species overlap, but they significantly differ in their CSA values. As a consequence, an analysis of both a MAS and a static NMR powder pattern spectrum is generally necessary for a reliable quantification of the $Q^{(n)}$ species (for a more precise way, see ref 58), as done, for example, in ref 56 for the NS4 glass.

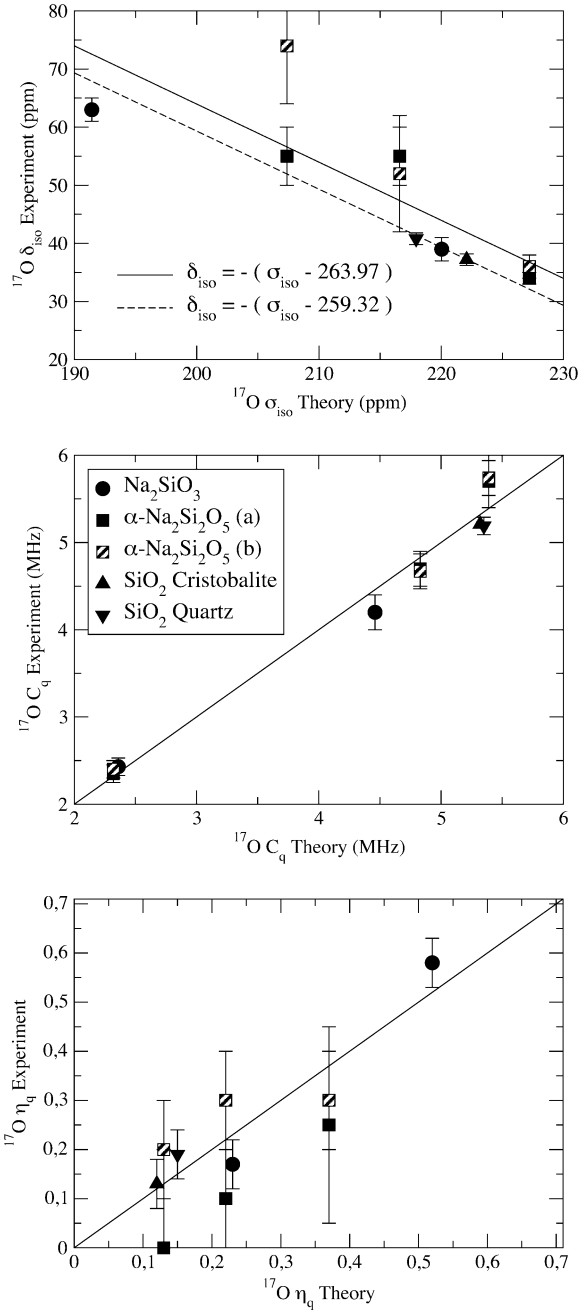


**Figure 2.** Experimental $^{17}$O NMR parameters versus theoretical values from Table 6. In the upper graph, the lines are linear fits with the constraint of unity slope; the solid line takes into account all data (correlation coefficient $R = 0.821$), while the dashed line is calculated without the BO α-$Na_2Si_2O_5$ data ($R = 0.991$). In the middle and bottom graphs, the solid line represents a perfect correspondence between theoretical and experimental values. [a]Ref 4, [b]ref 16.

**TABLE 9: $Q^{(n)}$ Composition of the Two Models of the Tetrasilicate Glass versus Experimental Values As Determined by NMR Spectroscopy**

| sample | $Q^{(2)}$ (%) | $Q^{(3)}$ (%) | $Q^{(4)}$ (%) |
|---|---|---|---|
| NS4 #1 | 8.33 | 33.33 | 58.33 |
| NS4 #2 | 4.17 | 41.67 | 54.17 |
| NS4 (#1 + #2) | 6.25 | 37.5 | 56.25 |
| NS4 (ref 56) | 6 | 40 | 54 |
| NS4 (ref 57) | 3 | 48 | 50 |

The mean values and the standard deviations of the theoretical NS4 $^{29}$Si NMR parameters are listed in Table 10. They are in good agreement with the experimental data reported in refs 56, 57. This is also shown by the comparison of the simulated static

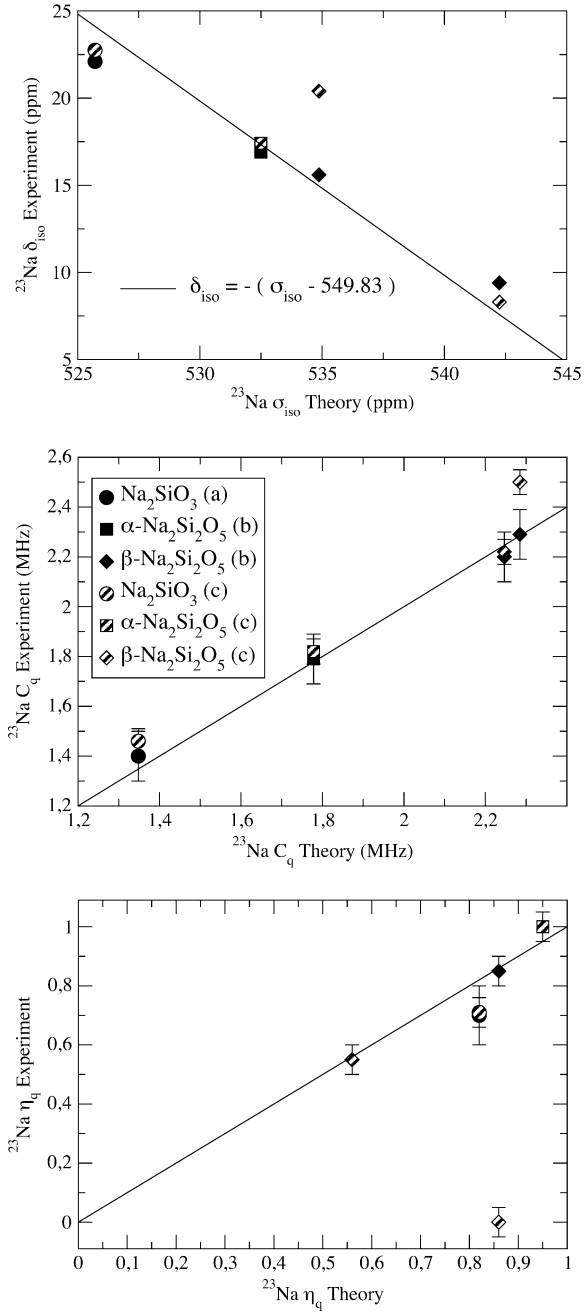


**Figure 3.** Experimental $^{23}$Na NMR parameters versus theoretical values from Table 7. The solid lines represent a perfect correspondence between theoretical and experimental values. [a]Ref 24, [b]ref 5, and [c]ref 6.

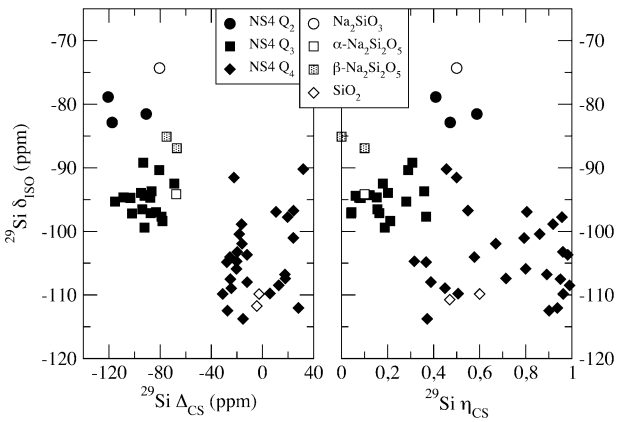


**Figure 4.** NS4 $^{29}$Si isotropic chemical shift $\delta_{iso}$ versus chemical shift anisotropy $\Delta_{cs}$ and asymmetry parameter $\eta_{cs}$. The theoretical data of the reference crystalline systems are also shown.

**TABLE 10: Experimental and Theoretical Mean Values (with standard deviations $\sigma$) of $^{29}$Si NMR Parameters of $Q^{(n)}$ Units in the Tetrasilicate Glass**

| | $\delta_{iso}$ (ppm) | | | | $\Delta_{cs}$ (ppm) | | | $\eta_{cs}$ | | |
|---|---|---|---|---|---|---|---|---|---|---|
| site | $\overline{\delta_{iso}}$ | $\sigma$ | $\delta_{iso}{}^a$ | $\delta_{iso}{}^b$ | $\overline{\Delta_{cs}}$ | $\sigma$ | $\Delta_{cs}{}^a$ | $\overline{\eta_{cs}}$ | $\sigma$ | $\eta_{cs}{}^a$ |
| $Q^{(2)}$ | −81.0 | 2.0 | −85 | −78.0 | −109.7 | 16.4 | −86 | 0.49 | 0.09 | 0.37 |
| $Q^{(3)}$ | −94.9 | 2.6 | −100 | −92.2 | −90.9 | 11.4 | −96 | 0.18 | 0.10 | 0 |
| $Q^{(4)}$ | −104.6 | 6.8 | −109 | −105.6 | −5.5 | 20.5 | 0 | 0.72 | 0.23 | 0 |

[a] Data from ref 56. [b] Data from ref 57.

and MAS spectra with the experimental ones displayed in Figure 5. The theoretical and experimental MAS spectra mainly differ in the relative intensities of the $Q^{(3)}$ and $Q^{(4)}$ peaks. This discrepancy may arise from the fact that the theoretical $\delta_{iso}$ distribution of the $Q^{(4)}$ seems broader than that of the $Q^{(3)}$, as a result of an insufficient sampling. This question should be addressed in a future work using models of greater size in order to improve our statistics as well as to investigate possible effects resulting from the finite size of the model.

*3.2.2. Oxygen-17.* The calculated NS4 $^{17}$O NMR parameters are displayed in Figure 6 and their mean values are listed in Table 11. The solid lines displayed in Figure 6 show some interesting trends between the NMR parameters which were obtained from linear regression analyses (in the remainder of the text, $R$ denotes the correlation coefficient):

$$\text{BO: } \delta_{iso} = 75.54 + 0.53\Delta_{cs}, \quad R = 0.575 \tag{4}$$

$$\text{NBO: } \delta_{iso} = 68.66 + 0.66\Delta_{cs}, \quad R = 0.531 \tag{5}$$

$$\text{BO: } \delta_{iso} = 94.02 - 8.43C_q, \quad R = 0.584 \tag{6}$$

$$\text{BO: } C_q = 3.34 - 0.038\Delta_{cs}, \quad R = 0.594 \tag{7}$$

$$\text{NBO: } C_q = 3.21 + 0.023\Delta_{cs}, \quad R = 0.459 \tag{8}$$

The NBO $\delta_{iso}$ is found to be not correlated to $C_q$ ($R = 0.319$). A noticeable characteristic of the $^{17}$O NMR parameters is the small scattering of both BO and NBO quadrupolar coupling constants $C_q$, and the strong overlap of their isotropic chemical

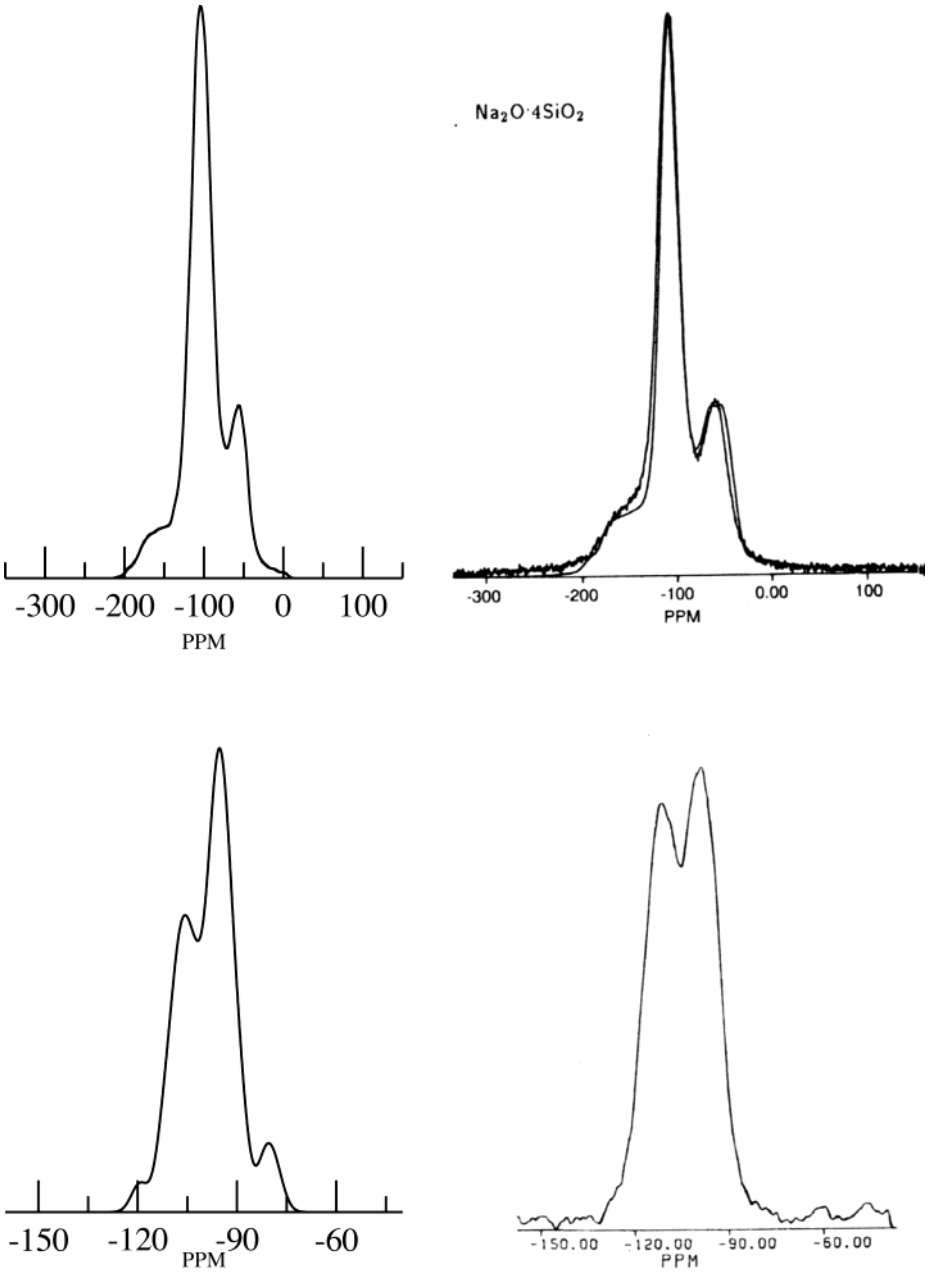


**Figure 5.** Simulated (left) and experimental (right), static (upper) and MAS (lower) $^{29}$Si NMR spectra of the tetrasilicate (NS4) glass. Experimental spectra are reprinted from ref 56. A 150 Hz Gaussian line broadening was applied to the theoretical data in order to smooth the simulated spectra.

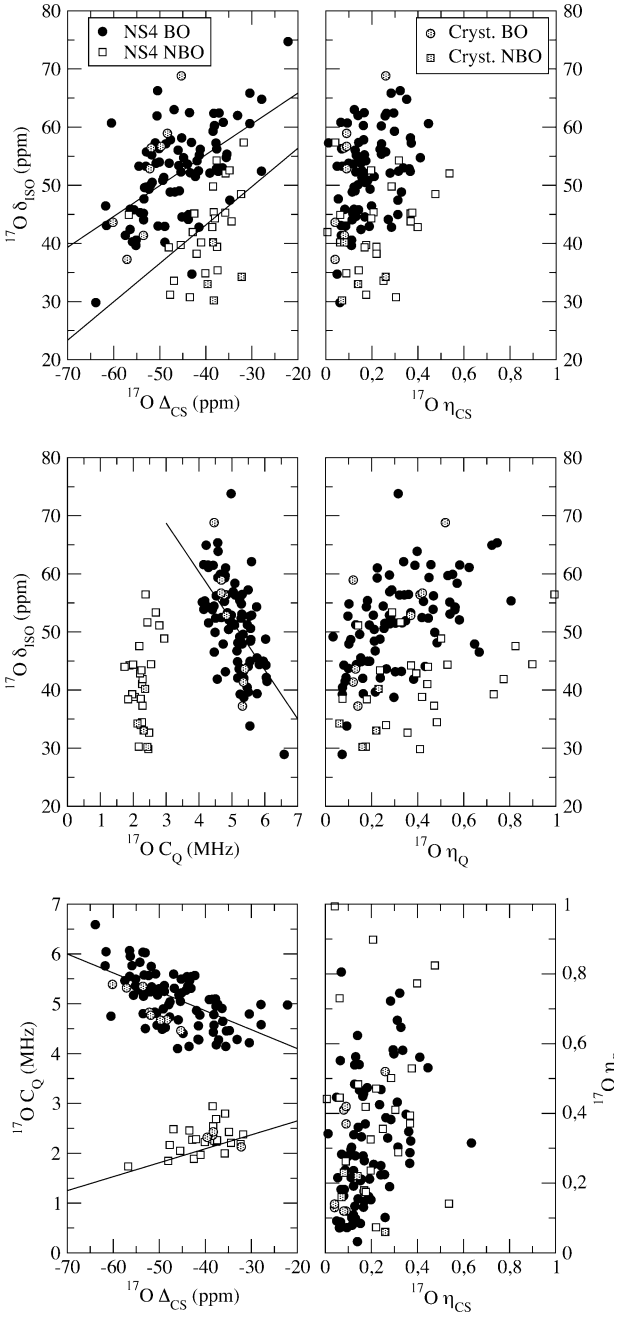


**Figure 6.** Theoretical $^{17}$O NMR parameters of the tetrasilicate (NS4) glass and of the crystalline compounds (see Table 6). The solid lines are linear fits taking into account NS4 data only (see eqs 4−8).

**TABLE 11: Theoretical Mean Values (with standard deviations $\sigma$) of the $^{17}$O NMR Parameters in the Tetrasilicate Glass**

| | $\delta_{iso}$ (ppm) | | $\Delta_{cs}$ (ppm) | | $\eta_{cs}$ | | $C_q$ (MHz) | | $\eta_q$ | |
|---|---|---|---|---|---|---|---|---|---|---|
| site | $\overline{\delta_{iso}}$ | $\sigma$ | $\overline{\Delta_{cs}}$ | $\sigma$ | $\overline{\eta_{cs}}$ | $\sigma$ | $\overline{C_q}$ | $\sigma$ | $\overline{\eta_q}$ | $\sigma$ |
| BO | 51.2 | 7.7 | −46.0 | 8.4 | 0.18 | 0.11 | 5.07 | 0.53 | 0.32 | 0.18 |
| NBO | 42.0 | 7.1 | −40.3 | 5.7 | 0.24 | 0.14 | 2.28 | 0.29 | 0.45 | 0.24 |

shift $\delta_{iso}$ range. This feature is extremely useful for the quantification of the BO/NBO ratio by NMR measurements. Indeed, whereas MAS NMR spectra often lack resolution (the BO and NBO lines strongly overlap, see the upper graph in Figure 7), the static powder pattern analysis provide unambiguous information as BO and NBO strongly differ in the strength of their *narrow-ranged* quadrupolar interaction $C_q$. This was done, for example, in refs 5 and16, but the $^{17}$O CSA is generally

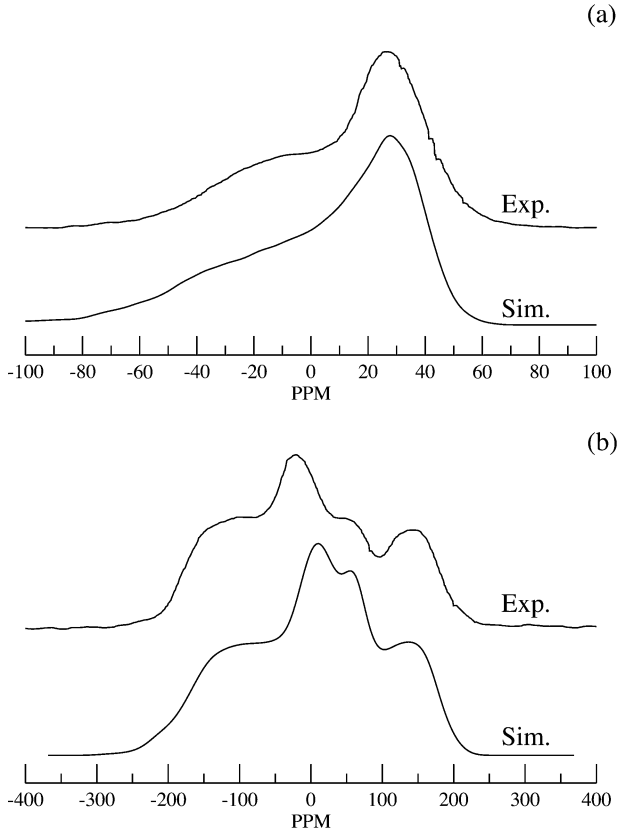


**Figure 7.** Simulated and experimental static (lower) and MAS (upper) $^{17}$O NMR spectra of the tetrasilicate (NS4) glass. Experimental spectra are reprinted from ref 4. A 150 Hz (respect. 650 Hz) Gaussian line broadening was applied to the theoretical data in order to smooth the simulated MAS (respect. static) spectrum.

ignored. For such a task, eqs 7and 8 could be useful in providing at least a rough estimate of the CSA, which is better than ignoring it.

Theoretical and experimental NMR spectra displayed in Figures 7 and 8 show good agreement between our predictions and experimental data. The simulation of the MQMAS spectra was done using an additional shift by 8 ppm of the $^{17}$O isotropic chemical shift, leading to $\sigma_{ref} = 251.32$ ppm. This could be explained from a different referencing procedure made in ref 53 (50% enriched-$^{17}$O water instead of tap-water was used for chemical shift reference). It is worth noticing that this parameter has no influence on the relative position of the BO and NBO lines, which agrees very well with the experimental ones.

*3.2.3. Sodium-23.* The calculated NS4 $^{23}$Na NMR parameters are shown in Figure 9, and the mean values with the standard deviations are listed in Table 12. In contrast to $^{29}$Si and $^{17}$O, the theoretical $^{23}$Na data are strongly scattered and it seems somewhat difficult to infer any trends from them. Comparison of simulated and experimental spectra (see Figure 10) shows a somewhat good agreement of the theoretical range of isotropic chemical shift $\delta_{iso}$ and quadrupolar interaction $C_q$ with experimental data. Indeed, the two isotropic projections (see the lower graph in the right panel of Figure 10) have the same chemical shift range. Discrepancies are mainly due to the insufficient number of sodium sites in our two NS4 models. Models of greater size will be investigated in future works.

## 4. Discussion

To investigate the structural significance of the NMR parameters, the coordination numbers of the sodium and oxygen

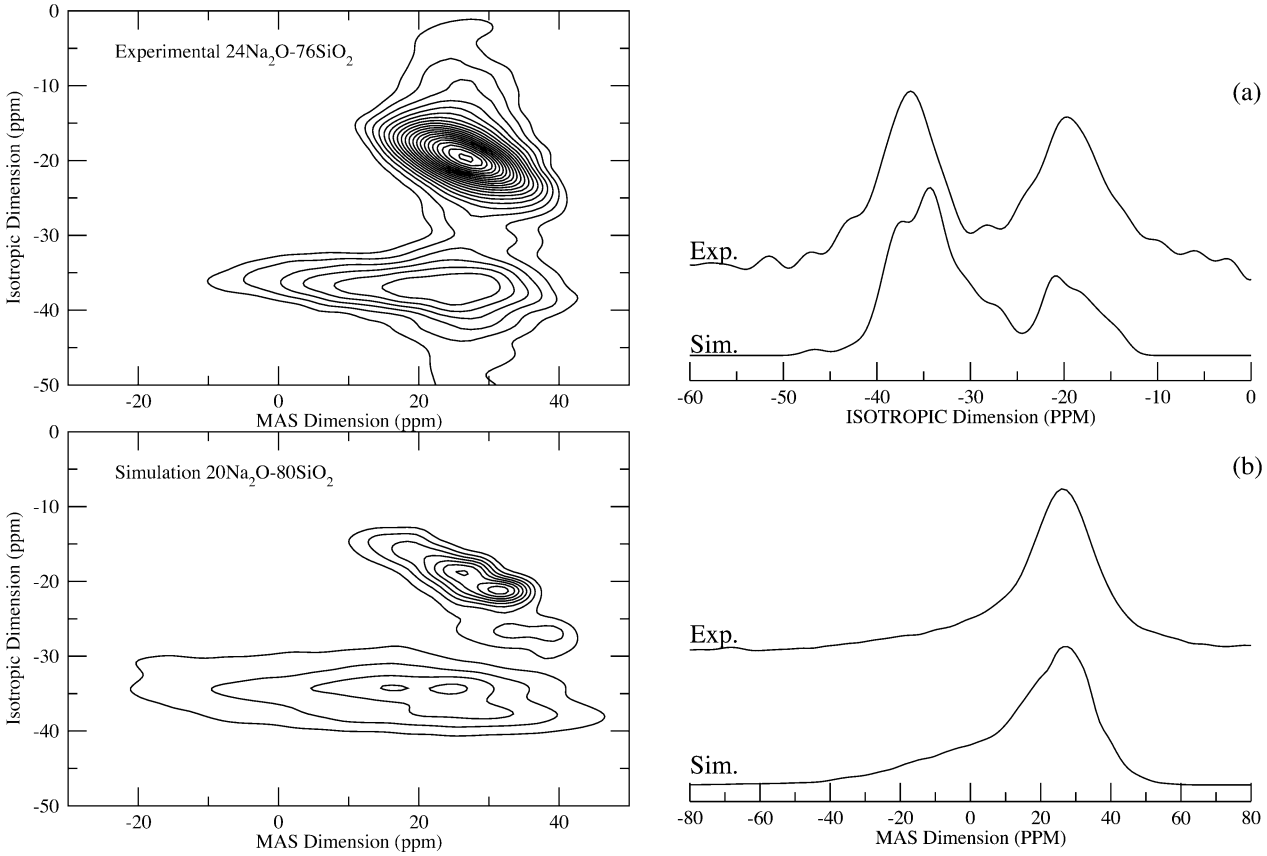


**Figure 8.** Simulated and experimental[53] MQMAS $^{17}O$ NMR spectra (left) and their projections (right) of sodosilicate glasses. The experimental data[53] corresponds to a sodosilicate glass containing 24% $Na_2O$. A 100 Hz (respect. 80 Hz) Gaussian line broadening was applied to the simulated MQMAS spectrum in the second (respect. first) dimension. The spectra were calculated using $\sigma_{ref} = 251.32$ ppm (see text).

atoms had to be determined. It was taken as the number of sodium atoms (respec. oxygen atoms) located in a sphere of 2.95 Å radius around each oxygen atoms (respec. sodium atoms). This radius was chosen according to the structural analysis of these sample presented in ref 59. Systematic linear regression analyses were performed between the NS4 (only) NMR parameters and structural factors such as bonding angles, distances, next nearest neighbors, and coordination numbers (see Table 1).

**4.1. Silicon-29.** The structural significance of $^{29}Si$ NMR parameters has been extensively studied and is well documented.[60] Besides the sensitivity to the connectivity of the silicate tetrahedra, the $^{29}Si$ isotropic chemical shift $\delta_{iso}$ is also known to be highly correlated to the mean $\langle Si-O-T\rangle$ angle, where T denotes a connected tetrahedron. But this dependence upon the intertetrahedral angle has been mostly studied for $Q^{(4)}$ species data whithin the framework of aluminosilicates.[60] Figure 11 is a plot of NS4 $^{29}Si$ isotropic chemical shift $\delta_{iso}$ against the mean $\langle Si-O-T\rangle$ angle. We found that the dependence of $\delta_{iso}$ upon $\langle Si-O-T\rangle$ is well described by means of the simple linear dependence:

$$T = Q^{(4)}:\ \delta_{iso} = -1.006\langle Si-O-T\rangle + 39.256, \quad R = 0.972 \tag{9}$$

$$T = Q^{(3)}:\ \delta_{iso} = -0.493\langle Si-O-T\rangle - 24.164, \quad R = 0.856 \tag{10}$$

$$T = Q^{(2)}:\ \delta_{iso} = -0.494\langle Si-O-T\rangle - 9.173, \quad R = 0.878 \tag{11}$$

These equations were obtained from a linear regression of the NS4 data only, but the crystalline data are also well described as shown in Figure 11. Among others, the relationship $\delta_{iso} = a + b\langle\cos(Si-O-T)\rangle$ gives slightly better results for $Q^{(3)}$ and $Q^{(2)}$ species:

$$T = Q^{(4)}:\ \delta_{iso} = 104.11\langle\cos(Si-O-T)\rangle - 24.39, \quad R = 0.971 \tag{12}$$

$$T = Q^{(3)}:\ \delta_{iso} = 54.87\langle\cos(Si-O-T)\rangle - 70.45, \quad R = 0.889 \tag{13}$$

$$T = Q^{(2)}:\ \delta_{iso} = 66.61\langle\cos(Si-O-T)\rangle - 94.61, \quad R = 0.974 \tag{14}$$

Further investigations were carried out only for $Q^{(4)}$ and $Q^{(3)}$ species, as the number of $Q^{(2)}$ sites is too small in our NS4 glass models to yield a reliable trend. For $Q^{(4)}$ species, we found an interesting trend connecting $\delta_{iso}$ to the number of sodium atoms to which the nearest neighbor (NN) oxygen atoms are coordinated, denoted as $N_{Na}$. Hence, $Q^{(4)}$ silicon sites follow the trend that $\delta_{iso}$ is increasing when $N_{Na}$ increases:

$$Q^{(4)}:\ \delta_{iso} = -111.13 + 3.347N_{Na}, \quad R = 0.621 \tag{15}$$

In fact, the above correlation can be related to the decrease of the $\langle Si-O-T\rangle$ angle with $N_{Na}$: $\langle Si-O-T\rangle = 148.615 - 2.892N_{Na}$ ($R = 0.556$). No (simple) relationship was found in order to describe the variation of the CSA parameters $\Delta_{cs}$ and $\eta_{cs}$ in the NS4 glass.

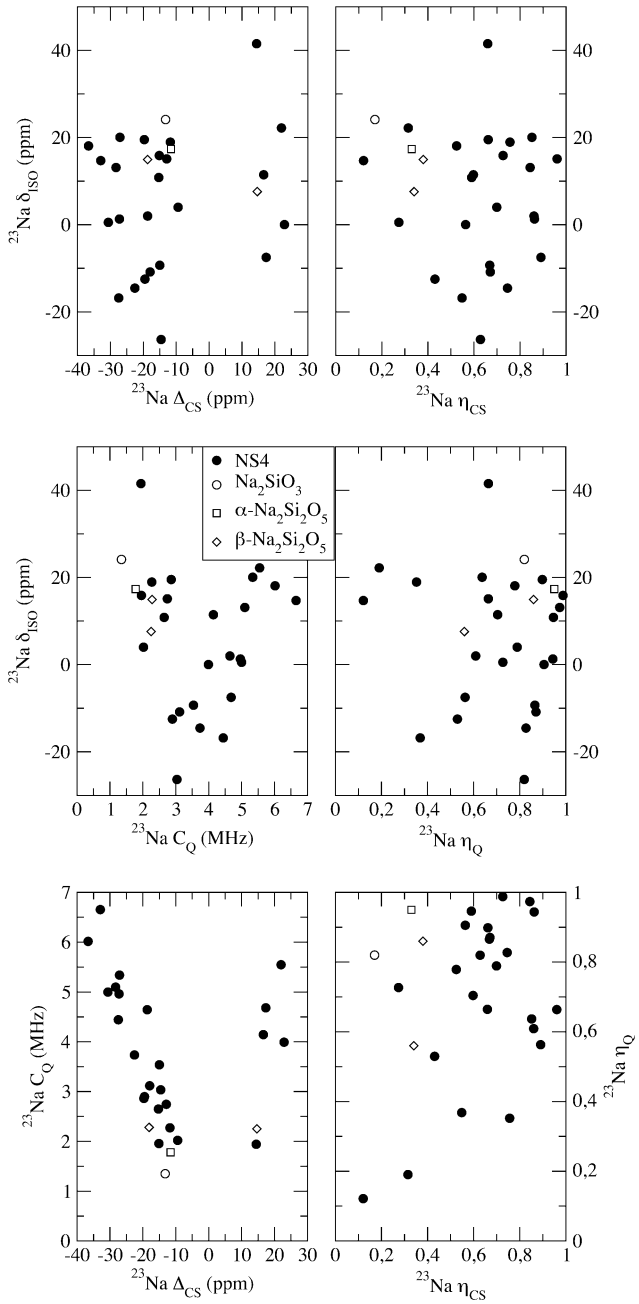


**Figure 9.** Theoretical $^{23}$Na NMR parameters of the tetrasilicate (NS4) glass and of the crystalline compounds (see Table 7).

For $Q^{(3)}$ species, interesting results were obtained for $\Delta_{cs}$. Denoting $N_{Si}$, the number of next nearest neighbor (NNN) silicon atoms ($N_{Si} = \sum_k n_k$ where $n_k$ is the speciation $Q^{(n_k)}$ of the $k$th silicon neighbor) and $N_{Na-NBO}$ the number of sodium atoms coordinated only to its nearest non bridging oxygens, the following correlations were obtained:

$$Q^{(3)}:\ \Delta_{cs} = -138.21 + 16.07N_{Na-NBO}, \quad R = 0.759 \quad (16)$$

$$Q^{(3)}:\ \Delta_{cs} = -111.75 + 4.64N_{Na}, \quad R = 0.507 \quad (17)$$

$$Q^{(3)}:\ \Delta_{cs} = -20.58 - 6.39N_{Si}, \quad R = 0.47 \quad (18)$$

The first relationship is certainly a consequence of the dependence of $\Delta_{cs}$ upon the Si−NBO (denoted $\langle Si-O\rangle_{NBO}$) bond length. Indeed, defining $\langle Si-O\rangle_{BO}$ as the mean Si−BO bond length, we obtained

**TABLE 12: Theoretical Mean Values (with standard deviations $\sigma$) of $^{23}$Na NMR Parameters in the Tetrasilicate Glass**

| $\delta_{iso}$ (ppm) | | $\Delta_{cs}$ (ppm) | | $\eta_{cs}$ | | $C_q$ (MHz) | | $\eta_q$ | |
|---|---|---|---|---|---|---|---|---|---|
| $\overline{\delta_{iso}}$ | $\sigma$ | $\overline{\Delta_{cs}}$ | $\sigma$ | $\overline{\eta_{cs}}$ | $\sigma$ | $\overline{C_q}$ | $\sigma$ | $\overline{\eta_q}$ | $\sigma$ |
| 5.47 | 15.76 | −12.90 | 17.98 | 0.64 | 0.20 | 3.89 | 1.36 | 0.70 | 0.24 |

$$Q^{(3)}:\ \Delta_{cs} = -1542.41 + 937.61\langle Si-O\rangle_{NBO}, \quad R = 0.790 \quad (19)$$

$$Q^{(3)}:\ \Delta_{cs} = 717.26 - 493.38\langle Si-O\rangle_{BO}, \quad R = 0.385 \quad (20)$$

This has lead us to perform a bilinear regression analysis which turns out to be quite successful, as shown in Figure 12 representing the relationship

$$Q^{(3)}:\ \Delta_{cs} = -733.09 - 494.65\langle Si-O\rangle_{BO} + 938.18\langle Si-O\rangle_{NBO}, \quad R = 0.879 \quad (21)$$

The coefficients were determined using NS4 data only, and Figure 12 shows that the crystalline data are rather well described by this empirical law. It should be mentioned that $\langle Si-O\rangle_{BO}$ and $\langle Si-O\rangle_{NBO}$ were found to be linearly independent ($R = 0.001$). Equation 21 shows that multivariable regression analysis may represent a fruitful approach for future investigations of simple parametric models.

**4.2. Oxygen-17.** During the past decade, a lot of attention has been devoted to the interpretation $^{17}$O NMR parameters.[4,13−15,20,21,23,24,29] It was suggested that bridging oxygens (BOs) may serve as a valuable probe of the $\langle Si-O-Si\rangle$ angle distribution. Several relationships have been proposed in order to describe the dependence of the BO quadrupolar coupling constant $C_q$ upon the $\langle Si-O-Si\rangle$ angle. Denoting $\Omega = \langle Si-O-Si\rangle$, we obtained the following results with the commonly used relationships:

$$C_q = 3.509\left(\frac{1}{2} + \frac{\cos\Omega}{\cos\Omega - 1}\right)^3 + 2.211, \quad R = 0.763 \quad (22)$$

$$C_q = 1.163 + 9.100\frac{\cos\Omega}{\cos\Omega - 1}, \quad R = 0.760 \quad (23)$$

$$C_q = 2.813 - 2.927\cos\Omega, \quad R = 0.764 \quad (24)$$

As shown in Figure 13 (upper graph), no clear influence of the number of coordinating sodiums can be inferred from these data. But influence of the geometry of the sodium atoms around each of the oxygen atoms has not yet been investigated.

We also attempted to take into account the $\langle Si-O\rangle$ bond length (denoted $\langle r\rangle$ beloow), yielding a slightly better fit using the following relatioinship:

$$C_q = 1.319\langle r\rangle^{2.888}\left(\frac{1}{2} + \frac{\cos\Omega}{\cos\Omega - 1}\right)^{2.179} + 0.511, \quad R = 0.807 \quad (25)$$

which shows an increase of $C_q$ with $\langle Si-O\rangle$ at constant bonding angle.

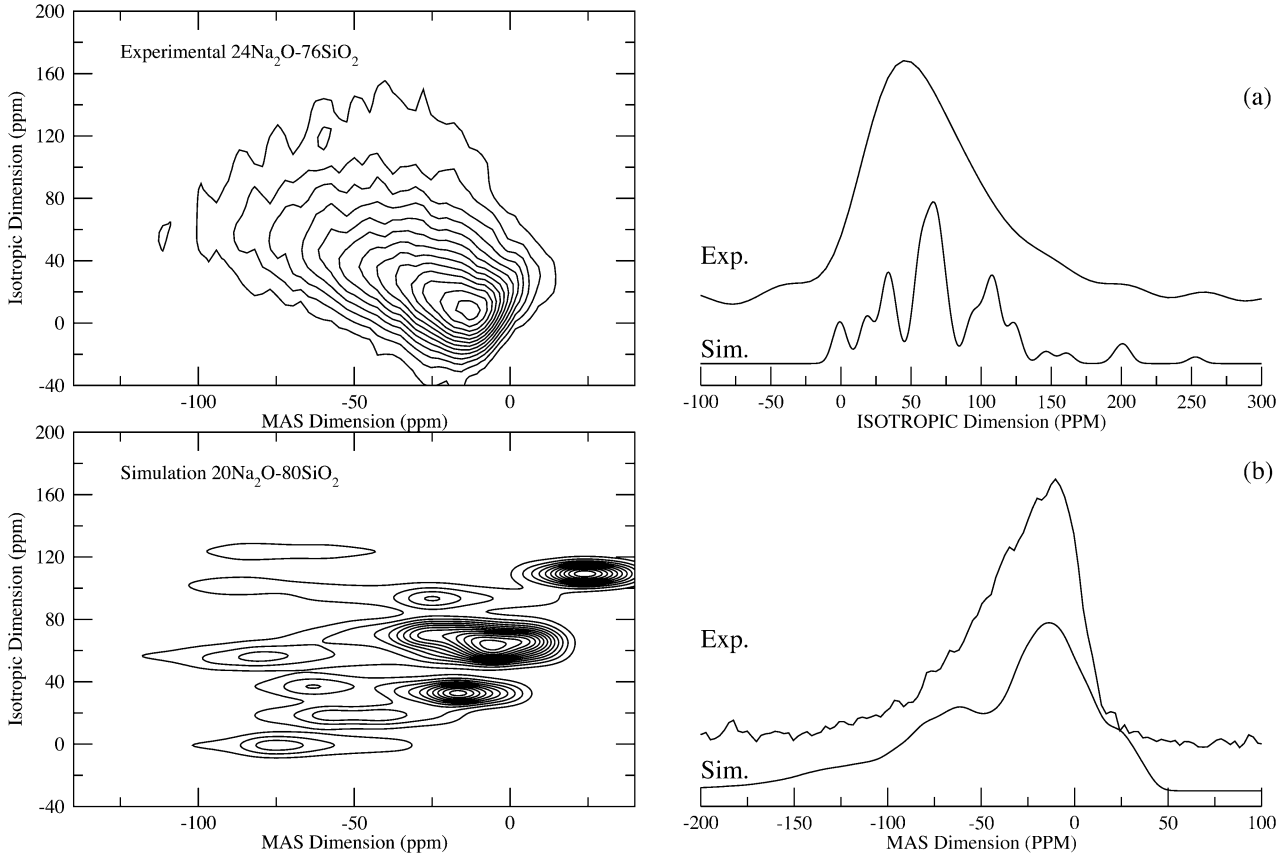


**Figure 10.** Simulated and experimental[53] MQMAS $^{23}$Na NMR spectra (left) and their projections (right) of sodosilicates glasses. The experimental data[53] correspond to a sodosilicate glass containing 24% $Na_2O$. A 100-Hz (respect. 80 Hz) Gaussian broadening was applied to the simulated MQMAS spectrum in the second (respect. first) dimension.

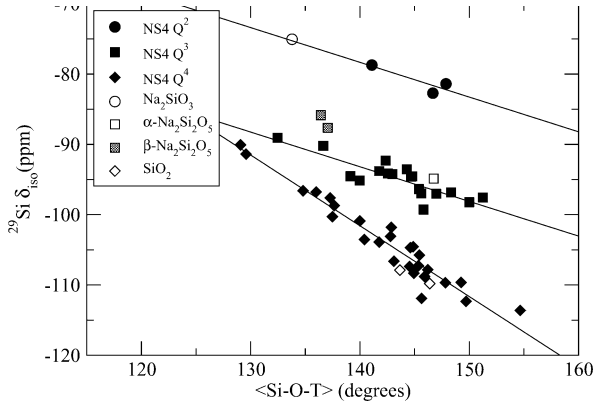


**Figure 11.** Theoretical $^{29}$Si isotropic chemical shift $\delta_{iso}$ as a function of the mean ⟨Si−O−T⟩ angle. The solid lines correspond to eqs 9 ($Q^{(4)}$), 10 ($Q^{(3)}$), and 11 ($Q^{(2)}$).

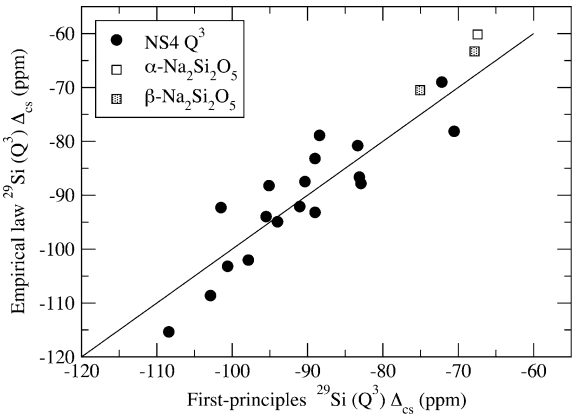


**Figure 12.** Calculated $Q^{(3)}$ $^{29}$Si chemical shift anisotropy $\Delta_{cs}$ according to the empirical law eq 21 versus (first-principles) theoretical values. The solid line represents a perfect correspondence.

Similarly to $C_q$, the results for the BO quadrupolar asymmetry parameter $\eta_q$ are From a combination of $C_q(\Omega)$ and $\eta_q(\Omega)$, one

$$\eta_q = 6.254\left(\frac{1}{2} + \frac{\cos\Omega}{\cos\Omega - 1}\right)^{1.332} + 0.128, \quad R = 0.823 \quad (26)$$

$$\eta_q = 1.752 - 3.316\frac{\cos\Omega}{\cos\Omega - 1}, \quad R = 0.817 \quad (27)$$

$$\eta_q = 1.131 - 1.051\cos\Omega, \quad R = 0.809 \quad (28)$$

expects a correlation between these two parameters as shown indeed in Figure 13:

$$C_q = 5.757 - 2.140\,\eta_q, \quad R = 0.726 \quad (29)$$

Nevertheless, from these data, no dependence upon the number of coordinating sodium atoms, like a different slope, is observed. This contradicts results of ref 24 using modeling clusters.

The analysis of the isotropic chemical shift did not provide significant correlations as shown in Figure 14, displaying the following relationships:

$$\delta_{iso} = 88.532 - 0.26\Omega, \quad R = 0.500 \quad (30)$$

$$\delta_{iso} = 81.964 - 4.26\mathrm{NNN}_{BO}, \quad R = 0.41 \quad (31)$$

where, $NNN_{BO}$ is the number of next nearest neighbor (NNN) bridging oxygen atoms. This corroborates the fact that the BO $^{17}$O isotropic chemical shift is dependent upon structural variation beyond the first coordination sphere.

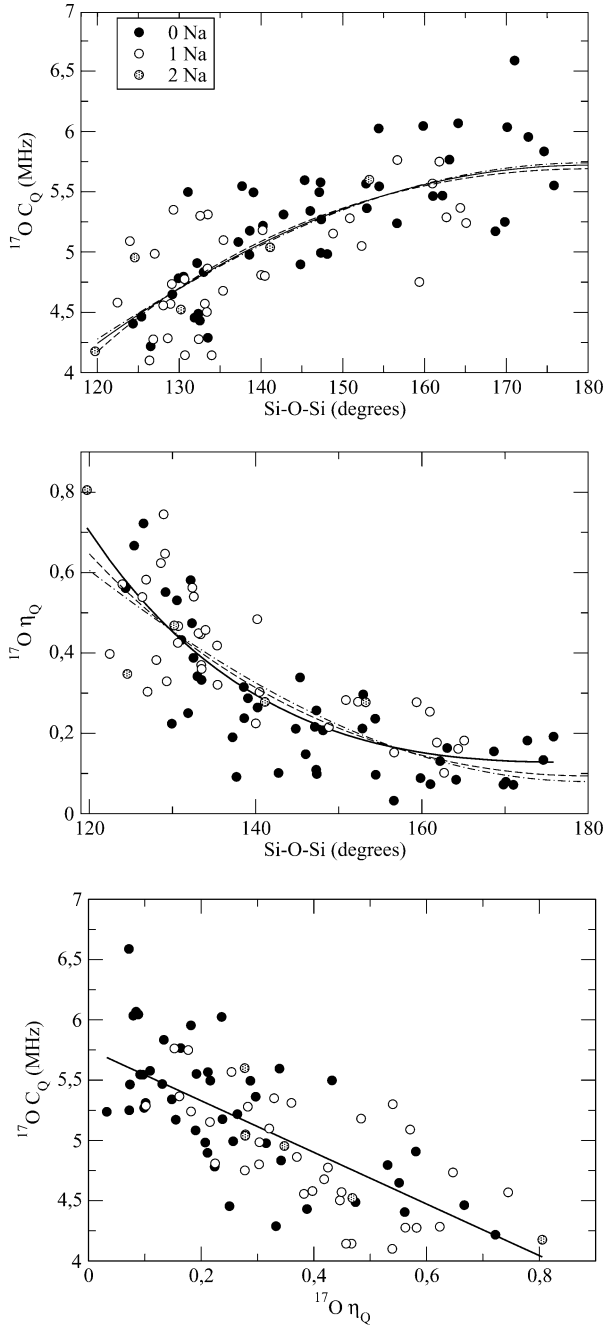


**Figure 13.** NS4 $^{17}$O (bridging oxygen) NMR quadrupolar parameters $C_q$ and $\eta_q$ versus the ⟨Si−O−Si⟩ angle. Oxygen atoms coordinated to no sodium cations are represented as filled circles, to one sodium atom as open circles, and to two sodium atoms as dashed circles. In the upper (respect. middle) graph, the solid line corresponds to eq 22 (respect. 26), the dashed line to eq 23 (respect. 27), and the dot−dashed line to eq 24 (respect. 28). In the lower graph, the solid line corresponds to eq 29.

Concerning the NBO, far fewer trends have been established so far, but also much less experimental data are available. For the present work, we have distinguished the NBO linked to a $Q^{(3)}$ and $Q^{(2)}$ silicon atom. These two species mainly differ in their ⟨Si−O⟩ bond length: the mean Si−NBO bond length for a $Q^{(2)}$ tetrahedron is 1.5662 Å ($\sigma = 0.0102$) while for a $Q^{(3)}$ is 1.5481 Å ($\sigma = 0.0096$). As shown in Figure 15, we observe that $C_q$ increases with the ⟨Si−O⟩ bond length

$$C_q = -15.876 + 11.689\langle \mathrm{Si{-}O}\rangle, \quad R = 0.500 \qquad (32)$$

whereas $\delta_{iso}$ seems to show no structural dependence upon this parameter. The influence of the geometry of the sodium atoms around each NBO has not been investigated, except for the coordination number, the mean ⟨Na−O⟩ distance and ⟨Si−O−Na⟩ angle for which no clear trends were observed.

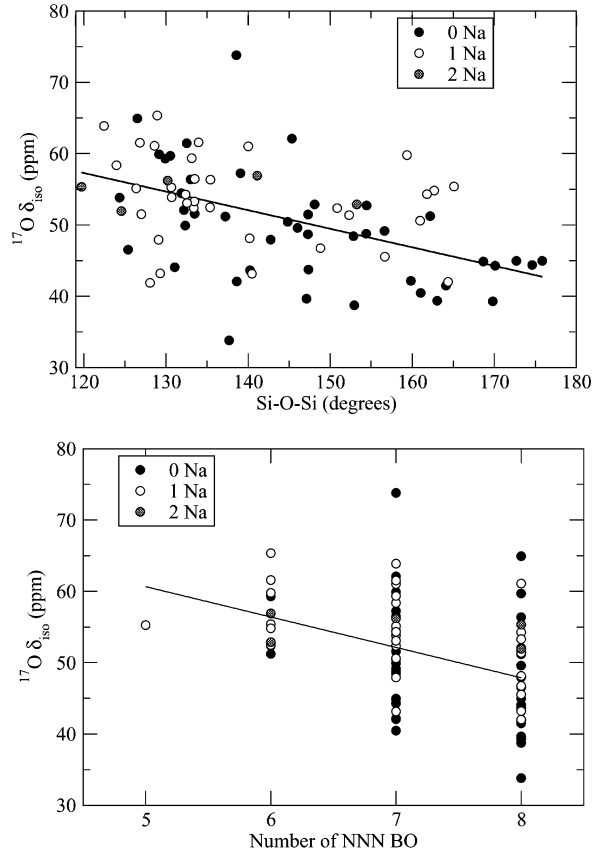


**Figure 14.** $^{17}$O (bridging oxygen) NMR isotropic chemical shift $\delta_{iso}$ versus the ⟨Si−O−Si⟩ angle (upper graph) and the number of next nearest neighbor bridging oxygen atoms (lower graph). Oxygen atoms coordinated to no sodium cations are represented as filled circles, to one sodium atom as open circles, and to two sodium atoms as dashed circles. The solid lines corresponds to eq 30 in the upper graph and to eq 31 in the lower graph.

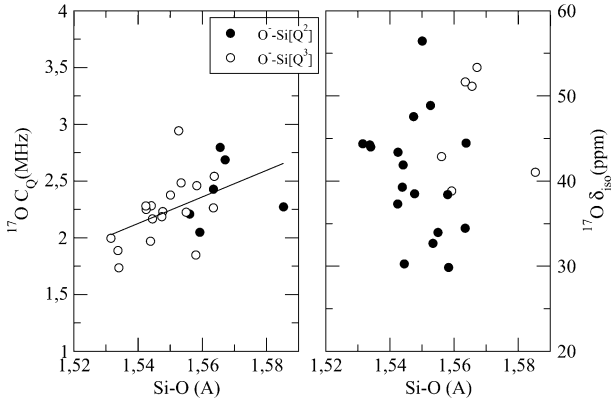


**Figure 15.** $^{17}$O non bridging oxygen NMR quadrupolar coupling constant $C_q$ (left graph) and isotropic chemical shift $\delta_{iso}$ (right graph) versus the ⟨Si−O⟩ bond length. Oxygen atoms coordinated to a $Q^{(2)}$ silicon atom are represented as filled circles and to a $Q^{(3)}$ silicon atom as open circles. In the left graph, the solid line corresponds to eq 32.

**4.3. Sodium-23.** There exist only very few investigations of the structural significance of $^{23}$Na NMR parameter in silicates.[5−9] In most of these works,[5,7−9] it was observed that $^{23}$Na isotropic chemical shift $\delta_{iso}$ decreases with increasing sodium coordination number and mean ⟨Na−O⟩ bond length, and decreases with

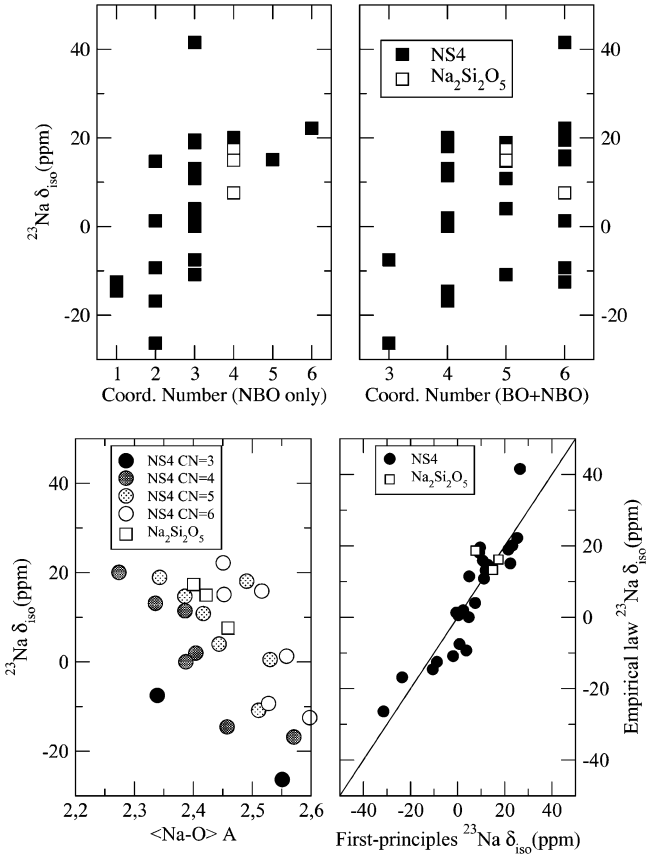


**Figure 16.** $^{23}$Na NMR isotropic chemical shift versus the number of coordinating non bridging oxygen atoms, the number of coordinating oxygen atoms, and the mean $\langle$Na$-$O$\rangle$ bond length. The lower right graph displays calculated isotropic chemical shift using eq 37 versus first-principles values; the solid line represents a perfect correspondence.

NBO/T (nonbridging oxygens per tetrahedrally coordinated cation). These trends are also observed for our data, as shown in Figure 16 where $^{23}$Na $\delta_{iso}$ is found to be best correlated to the number of coordinating non bridging oxygen atoms ($N_{NBO}$), rather than the number of coordinating bridging oxygen atoms ($N_{BO}$) or the number of coordinating oxygen atoms ($N_O$):

$$\delta_{iso} = -19.740 + 8.52287N_{NBO}, \quad R = 0.607 \quad (33)$$

$$\delta_{iso} = 9.360 - 2.12042N_{BO}, \quad R = 0.185 \quad (34)$$

$$\delta_{iso} = -25.511 + 6.46635N_{O}, \quad R = 0.419 \quad (35)$$

In Figure 16 (lower graph), we can observe the trend of decreasing $^{23}$Na $\delta_{iso}$ with increasing mean $\langle$Na$-$O$\rangle$ bond length, as a function of the coordination number. The slope of the decrease is roughly equal for all coordination numbers, and $\delta_{iso}$ is approximately shifted by 10 ppm when the coordination number increases by one. The main contribution of the scatter of these data may be related to the arbitrariness of the Na coordination numbers. Indeed, for some $^{23}$Na sites in our samples, the first oxygen coordination sphere is rather ill defined. Despite this difficulty, the above trends can be defined through the linear relationships

$$\delta_{iso} = 335.99 - 158.59\langle Na{-}O\rangle + 11.82N_{O}, \quad R = 0.892 \quad (36)$$

$$\delta_{iso} = 286.29 - 139.18\langle Na{-}O\rangle + 10.62N_{BO} + 13.35N_{NBO}, \quad R = 0.907 \quad (37)$$

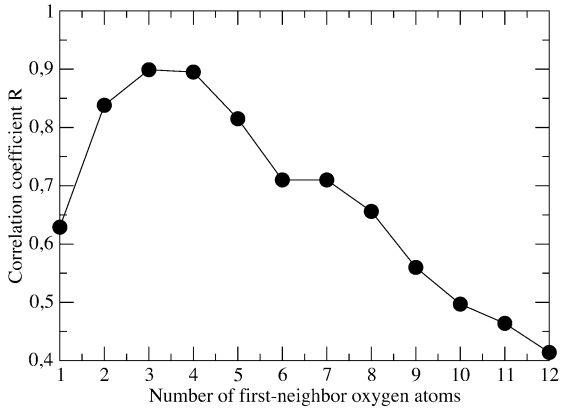


**Figure 17.** Correlation coefficient $R$ of the regression between the $^{23}$Na NMR isotropic chemical shift and the average $\langle$Na$-$O$\rangle_N$ distance, versus $N$, the number of first-neighbor oxygen atoms used to calculate $\langle$Na$-$O$\rangle_N$.

which describes rather well our data, as shown in Figure 16 for eq 37. As an alternative approach for correlating $\delta_{iso}$ to the Na$-$O bond length, we performed regressions between $\delta_{iso}$ and the average $\langle$Na$-$O$\rangle_N$ distance calculated with the N first-neighbor oxygen atoms. As shown in Figure 17, best correlations are obtained when considering three or four oxygen atoms:

$$\delta_{iso} = -173.23\langle Na{-}O\rangle_3 + 411.22, \quad R = 0.899 \quad (38)$$

$$\delta_{iso} = -138.95\langle Na{-}O\rangle_4 + 339.61, \quad R = 0.895 \quad (39)$$

Thus, despite the dependence of the $^{23}$Na isotropic chemical shift with its coordination number, it can serve as a valuable probe of the mean Na$-$O bond length, as applied in refs 9,18.

Concerning the quadrupole interaction, no clear and simple trend could be obtained from our data and probably deeper investigation is required.

## 5. Summary and Conclusions

Using sodium silicates compounds of known structure and NMR parameters, we have shown that the first-principles GIPAW method can predict with accuracy the $^{29}$Si, $^{17}$O, and $^{23}$Na NMR chemical shielding tensors and quadrupolar coupling parameters, in sodosilicates systems. Using a supercell approach, we have also shown that the GIPAW method can also be applied to amorphous silicates, using models generated by molecular dynamics. In contrast to previous studies using modeling clusters, this approach probably better accounts for the local environnement that exists in real systems. The GIPAW method is more efficient regarding scaling properties with the size of the system under study.

In the present work, we have considered the sodium tetrasilicate glass, and $^{29}$Si, $^{17}$O, and $^{23}$Na theoretical NMR spectra were in good agreement with the experimental data. Based on these results, we have investigated the relationships between the NMR and the structural parameters that exit in such glassy systems. For $^{29}$Si, a linear dependence of the $Q^{(4)}$, $Q^{(3)}$, and $Q^{(2)}$ isotropic chemical shift with the mean $\langle$Si$-$O$-$T$\rangle$ angle has been obtained, in agreement with the results of the literature. We have also shown that the $Q^{(3)}$ chemical shift anisotropy can be well predicted by a simple linear function of the $\langle$Si$-$O$\rangle_{BO}$ and $\langle$Si$-$O$\rangle_{NBO}$ bond length, with errors less than 10 ppm. For bridging oxygens, the quadrupolar coupling constant $C_q$ and asymmetry parameter $\eta_q$ are primarly influenced by the

⟨Si−O−Si⟩ angle. This dependence can be described by relationships previously derived from ab initio calculations using modeling clusters. However, no clear influence of the coordinating sodium on the quadrupolar parameters could be established. We have also observed that the isotropic chemical shift could not be simply related to structural parameters of the first and second coordination sphere, as well as for non briding oxygens. But the NBO quadrupolar coupling constant increases, on average, with the ⟨Si−O⟩ bond length. More quantitative analysis which requires a larger set of data will be performed in future works. For sodiums, only the isotropic chemical shift displays clear trends such as its increase with the number of coordinating non bridging oxygen atoms to a given Na or its decrease with the mean ⟨Na−O⟩ bond length in an approximately linear manner. As a linear function of the ⟨Na−O⟩, the number of coordinating bridging and nonbridging oxygens, the $^{23}$Na isotropic chemical shift can be predicted with errors less than 10 ppm. These relationships also corroborate the influence of the bonding character of the coordinating oxygen atoms.

For all these nuclei, we have also investigated trends between the NMR parameters themselves. They probably result from relationships between the structural parameters that can be reproduced by our models, or more generally by the use of molecular dynamics models. We expect that such relationships will simplify the problem of extracting the distributions of NMR parameters from experimental data by reducing the number of unknowns.

Finally, this work opens exciting perspectives concerning the combination of molecular dynamics with prediction of NMR properties of periodic systems. It also offers a promising alternative to the traditional clusters approach.

**Acknowledgment.** We thank Magali Benoit for very interesting and stimulating discussions. The Car-Parrinello simulations have been performed on the IBM/SP3 in CiNES, Montpellier, France. The NMR calculations were performed on the Compaq SC256 parallel computer of CEA Grenoble under grand p556.

## Appendix

**Relaxed Crystalline Structures.** The parameters of the relaxed structure of the $Na_2SiO_3$, α-$Na_2Si_2O_5$, and β-$Na_2Si_2O_5$ are given in Tables 13, 14, and 15, respectively.

**TABLE 13: Upper: Atomic Coordinates of the Sodium Metasilicate Structure Obtained after Relaxation. The Symmetry of the Crystal Is *Cmc*2$_1$ and the Primitive Cell Has Been Used in Calculations. Lower: Lattice Parameters (in au) of the Sodium Metasilicate Scaled so As To Span the Experimental Unit Cell Volume**

| Atomic Coordinates | | | |
|---|---|---|---|
| atom | *x* | *y* | *z* |
| Na | 0.50445 | −0.17342 | 0.00007 |
| Si | 0.15760 | −0.15760 | 0.53602 |
| O(1) | 0.41590 | −0.15797 | 0.48140 |
| O(2) | 0.08367 | −0.08367 | 0.87216 |
| **Lattice Parameters** | | | |
| lattice vector | *x* | *y* | *z* |
| **a** | 11.44320 | 0.01155 | 0 |
| **b** | 5.69413 | 9.92592 | 0 |
| **c** | 0 | 0 | 9.10848 |

**TABLE 14: Upper: Atomic Coordinates of the Sodium Disilicate-α Structure Obtained after Relaxation. The Symmetry of the Crystal Is *Pcnb*. Lower: Lattice Parameters (in au) of the Sodium Disilicate-α Scaled So As To Span the Experimental Unit Cell Volume**

| Atomic Coordinates | | | |
|---|---|---|---|
| atom | *x* | *y* | *z* |
| Na | 0.09786 | 0.56045 | 0.23711 |
| Si | 0.10508 | 0.34287 | 0.29576 |
| O(1) | 0.00000 | 0.25000 | 0.24084 |
| O(2) | 0.18076 | 0.34736 | 0.61512 |
| O(3) | −0.04634 | 0.42130 | 0.24020 |
| **Lattice Parameters** | | | |
| lattice vector | *x* | *y* | *z* |
| **a** | 12.10728 | 0 | 0 |
| **b** | 0 | 29.15514 | 0 |
| **c** | 0 | 0 | 9.25141 |

**TABLE 15: Upper: Atomic Coordinates of the Sodium Disilicate-β Structure Obtained after Relaxation. The Symmetry of the Crystal Is *P*2$_1$/*c*. Lower: Lattice Parameters (in au) of the Sodium Disilicate-β Scaled So As To Span the Experimental Unit Cell Volume**

| Atomic Coordinates | | | |
|---|---|---|---|
| atom | *x* | *y* | *z* |
| Na | 0.37917 | 0.75287 | 0.44210 |
| Na | 0.13635 | 0.22554 | 0.47221 |
| Si | 0.02789 | 0.18558 | 0.18290 |
| Si | 0.40310 | 0.29386 | 0.27684 |
| O(1) | 0.01535 | −0.13910 | 0.21512 |
| O(2) | 0.45475 | 0.61770 | 0.26704 |
| O(3) | 0.22565 | 0.24576 | 0.18171 |
| O(4) | 0.39139 | 0.23200 | 0.40018 |
| O(5) | −0.09214 | 0.24453 | 0.06492 |
| **Lattice Parameters** | | | |
| lattice vector | *x* | *y* | *z* |
| **a** | 15.34237 | 0 | −0.001787 |
| **b** | 0 | 6.16696 | 0 |
| **c** | −5.72369 | 0 | 22.60890 |

## References and Notes

(1) Mägi, M.; Lippmaa, E.; Samoson, A. *J. Phys. Chem.* **1984**, *88*, 1518.
(2) Mueller, K.; Wu, Y.; Chmelka, B.; Stebbins, J. F.; Pines, A. *J. Am. Chem. Soc.* **1991**, *113*, 32.
(3) Mueller, K.; Baltisberger, J.; Wooten, E.; Pines, A. *J. Phys. Chem.* **1992**, *96*, 7001.
(4) Xue, X.; Stebbins, J. F.; Kanzaki, M. *Am. Mineral.* **1994**, *79*, 31.
(5) Xue, X.; Stebbins, J. F. *Phys. Chem. Miner.* **1993**, *20*, 297.
(6) Koller, H.; Engelhardt, G.; Kentgens, A.; Sauer, J. *J. Phys. Chem.* **1994**, *98*, 1544.
(7) George, A. M.; Stebbins, J. F. *Am. Mineral.* **1995**, *80*, 878.
(8) Stebbins, J. F. *Solid State Ionics* **1998**, *80*, 878.
(9) Lee, S.; Stebbins, J. F. *Geochim. Cosmochim. Acta* **2003**, *67*, 1699.
(10) Tossell, J.; Lazzaretti, P. *Chem. Phys.* **1987**, *112*, 205.
(11) Tossell, J.; Lazzaretti, P. *Phys. Chem. Miner.* **1988**, *15*, 564.
(12) Tossell, J. *J. Non-Cryst. Solids* **1990**, *13*, 120.
(13) Lindsay, C.; Tossell, J. *Phys. Chem. Miner.* **1991**, *18*, 191.
(14) Sternberg, U. *Solid State NMR* **1993**, *2*, 181.
(15) Grandinetti, P.; Baltisberger, J.; Farnan, I.; Stebbins, J. F.; Werner, U.; Pines, A. *J. Phys. Chem.* **1995**, *99*, 12341.
(16) Maekawa, H.; Florian, P.; Massiot, D.; Kiyono, H.; Nakaruma, M. *J. Phys. Chem.* **1996**, *100*, 5525.
(17) Farnan, I.; Grandinetti, P. J.; Baltisberger, J. H.; Stebbins, J. F.; Werner, U.; Eastman, M. A.; Pines, A. *Nature* **1992**, *358*, 31.
(18) Angeli, F.; Delaye, J.-M.; Charpentier, T.; Petit, J.-C.; Ghaleb, D.; Faucon, P. *J. Non-Cryst. Solids* **2000**, *276*, 132.
(19) Angeli, F.; Delaye, J.-M.; Charpentier, T.; Petit, J.-C.; Ghaleb, D.; Faucon, P. *Chem. Phys. Lett.* **2000**, *320*, 681.

(20) Vermillion, K.; Florian, P.; Grandinetti, P. *J. Chem. Phys.* **1998**, *108*, 7274.
(21) Xue, X.; Kanzaki, M. *Phys. Chem. Miner.* **1998**, *26*, 14.
(22) Xue, X.; Kanzaki, M. *J. Phys. Chem. B* **1999**, *103*, 10816.
(23) Xue, X.; Kanzaki, M. *Solid State NMR* **2000**, *16*, 245.
(24) Clark, T.; Grandinetti, P.; Florian, P.; Stebbins, J. F. *J. Phys. Chem.* **2001**, *105*, 12257.
(25) Tossell, J. *Phys. Chem. Miner.* **1999**, *27*, 70.
(26) Pickard, C.; Mauri, F. *Phys. Rev. B* **2001**, *63*, 245101.
(27) Blöchl, P. *Phys. Rev. B* **1994**, *50*, 17953.
(28) Petrilli, H.; Blöchl, P.; Blaha, P.; Schwarz, K. *Phys. Rev. B* **1998**, *57*, 14690.
(29) Profeta, M.; Mauri, F.; Pickard, C. *J. Am. Chem. Soc.* **2003**, *125*, 541.
(30) Mauri, F.; Pfrommer, B.; Louie, S. *Phys. Rev. Lett.* **1996**, *77*, 5300.
(31) Mauri, F.; Pfrommer, B.; Louie, S. *Phys. Rev. Lett.* **1997**, *79*, 2340.
(32) Perdew, J.; Burke, K.; Ernzerhof, M. *Phys. Rev. Lett.* **1996**, *77*, 3865.
(33) Trouiller, N.; Martins, J. *Phys. Rev. B* **1991**, *43*, 1993.
(34) Kleiman, L.; Bylander, D. *Phys. Rev. Lett.* **1982**, *48*, 1425.
(35) Monkhorst, H. J.; Pack, J. D. *J. P. Phys. Rev. B* **1976**, *13*, 5188.
(36) Pfrommer, B.; Raczkowski, D.; Canning, A.; Louie, S. G., Lawrence Berkeley National Laboratory, "PARAllel Total Energy Code" (PARATEC) With contributions from Mauri, F.; Cote, M.; Yoon, Y.; Pickard, C. J.; Haynes, P. For more information see: http://www.nersc.gov/projects/paratec/.
(37) Mehring, M. *High-resolution NMR spectroscopy in solids*; Springer-Verlag: Berlin, 1976.
(38) Pyykkö, P. *Mol. Phys.* **2001**, *99*, 1617.
(39) Bansal, N. P.; Doremus, R. H. *Handbook of Glass Properties*; Academic Press: Inc.: New York, 1986.
(40) Benoit, M.; Ispas, S.; Jund, P.; Jullien, R. *Eur. Phys.* **2000**, *13*, 631.
(41) Benoit, M.; Kob, W. *Europhys. Lett.* **2002**, *60*, 269.
(42) Ispas, S.; Benoit, M.; Jund, P.; Jullien, R. *Phys. Rev. B* **2001**, *64*, 214206.
(43) Ispas, S.; Benoit, M.; Jund, P.; Jullien, R. *J. Non. Cryst. Solids* **2002**, *307*−*310*, 946.
(44) Kramer, G. J.; de Man, A. J. M.; van Santen, R. A. *J. Am. Chem. Soc.* **1991**, *113*, 6435.
(45) Horbach, J.; Kob, W.; Binder, K. *Chem. Geol.* **2001**, *174*, 87.
(46) Jund, P.; Kob, W.; Jullien, R. *Phys. Rev. B* **2001**, *64*, 134303.
(47) Sunyer, E.; Jund, P.; Jullien, R. *Phys. Rev. B* **2002**, *65*, 214203.
(48) Horbach, J.; Kob, W.; Binder, K. *Phys. Rev. Lett.* **2002**, *88*, 125502.
(49) Car, R.; Parrinello, M. *Phys. Rev. Lett.* **1985**, *55*, 2471.
(50) Marx, D.; Hutter, J.Forschungszentrum Jülich, NIC Series; Grotendorst, J., Ed.; 2000; Vol.1.
(51) Hutter, J.; Alavi, A.; Deutsch, T.; Bernasconi, M.; Goedecker, S.; Marx, D.; Tuckerman, M.; Parrinello, M. "CPMD Version 3.3, MPI für Festkörperforschung and IBM Research (1995−1999)".
(52) Charpentier, T.; Fermon, C.; Virlet, J. *J. Chem. Phys.* **1998**, *109*, 3116.
(53) Angeli, F. Structure et réactivité aqueuse des verres silicatés. Apport de la résonance magnétique nucléaire haute-résolution, Thesis, Université Paris VII, 2000.
(54) Angeli, F.; Charpentier, T.; Gin, S.; Petit, J. *Chem. Phys. Lett.* **2001**, *341*, 23.
(55) Heidemann, D.; Huebert, C.; Schwieger, W.; Grabner, P.; Bergk, K.-H.; Sarv, P. *Z. Anorg. Allg. Chem.* **1992**, *617*, 169.
(56) Emerson, J.; Stallworth, P.; Bray, P. *J. Non-Cryst. Solids* **1989**, *113*, 253.
(57) Maekawa, H.; Maekawa, T.; Kawamura, K.; Yokokawa, T. *J. Non-Cryst. Solids* **1991**, *127*, 53.
(58) Zhang, P.; Dunlap, C.; Florian, P.; Grandinetti, P.; Farnan, I.; Stebbins, J. F. *J. Non-Cryst. Solids* **1996**, *204*, 294.
(59) Ispas, S.; Benoit, M.; Jund, P.; Jullien, R. *Phys. Rev. B* **2001**, *64*, 214206.
(60) Engelhardt, G.; Michel, D. *High-resolution solid-state NMR spectroscopy of silicates and zeolites*; Wiley: New York, 1987.
(61) McDonald, W.; Cruickshank, D. *Acta Crystallogr.* **1967**, *22*, 37.
(62) Pant, A.; Cruickshank, D. *Acta Crystallogr.* **1968**, *B24*, 13.
(63) Pant, A. *Acta Crystallogr.* **1968**, *B24*, 1077.
(64) Spearing, D. R.; Farnan, I.; Stebbins, J. F. *Phys. Chem. Miner.* **1992**, *19*, 307.
(65) Larsen, F. H.; Farnan, I. *Chem. Phys. Lett.* **2002**, *357*, 403.
(66) Spearing, D. R.; Stebbins, J. F. *Am. Mineral.* **1989**, *74*, 956.